APPLICATION OF ELECTROCHEMICAL METHODS IN WASTEWATER TREATMENT: DESORPTION AND RECOVERY OF ZINC

FOONG KOK CHONG

A project report submitted in partial fulfilment of the requirements for the award of Bachelor of Engineering (Hons.) Chemical Engineering

Faculty of Engineering and Science
Universiti Tunku Abdul Rahman

April 2015

DECLARATION

I hereby declare that this project report is based on my original work except for citations and quotations which have been duly acknowledged. I also declare that it has not been previously and concurrently submitted for any other degree or award at UTAR or other institutions.

Signature : CHONG

Name : Foong Kok Chong

ID No. : 10 UEB 03948

Date : 7 May 2015

APPROVAL FOR SUBMISSION

I certify that this project report entitled **"APPLICATION OF ELECTROCHEMICAL METHODS IN WASTEWATER TREATMENT: DESORPTION AND RECOVERY OF ZINC"** was prepared by **FOONG KOK CHONG** has met the required standard for submission in partial fulfilment of the requirements for the award of Bachelor of Engineering (Hons.) Chemical Engineering at Universiti Tunku Abdul Rahman.

Approved by,

Signature : _____

Supervisor : Dr Gulnaziya Issabayeva

Date : _____

ACKNOWLEDGEMENTS

I appreciate UTAR for offering final year project to all engineering students. This final year project has provided me an excellent platform to apply science and engineering knowledge in my research project.

My sincere thank to Dr. Gulnaziya Issabayeva for accepting me as her final year project student. Above and beyond, I owe my final year project supervisor, an earnest acknowledgement in mentoring me with my final year project. I am grateful to each and every advice offered to me by UTAR laboratory officers in assisting my research experiment. My coursemates who have lent a hand in my research project, deserve the very last credit and merit.

APPLICATION OF ELECTROCHEMICAL METHODS IN WASTEWATER TREATMENT: DESORPTION AND RECOVERY OF ZINC

ABSTRACT

This research project studied the desorption and recovery of zinc from wastewater by electrochemical method. Zinc ions in synthetic solution were removed by adsorption onto palm shell activated carbon in batch adsorption. 10 % hydrochloric acid was used as the desorbing agent to extract zinc ions out from activated carbon in batch desorption, which showed desorption efficiency in the range of 20 to 23 %. The desorption solution was subjected to cyclic voltammetry and chronoamperometry experiments to study zinc electrodeposition. Cyclic voltammetry experiment determined that the electrodeposition potential of zinc was +1.297 V. The parameters that influenced the recovery process, i.e. control electrolyte, conductivity salt, pH buffer, electrolyte pH, electrolyte temperature and pulse current, were varied in each test. This research project demonstrated that electrolyte pH at 4.5 achieved 100 % zinc recovery after 15 minutes, while electrolyte solution containing 1.0 M potassium chloride conductivity salt attained 62.19 % zinc recovery in 60 minutes. The results also proposed that zinc electrodeposition occurred through dissociation of anionic zincate complexes that released free zinc ions for reduction at the working electrode. On the contrary, control electrolyte, boric acid, electrolyte temperature at 45 ^{o}C and pulse current exhibited 0 % zinc recovery, due to the presence of stable coordination complexes and molecules that strongly bound zinc ions and inhibited zinc electrodeposition.

TABLE OF CONTENTS

LIST OF TABLES

LIST OF FIGURES

LIST OF SYMBOLS / ABBREVIATIONS

C	Concentration, M
E_0	Standard electrode potential, V
I	Current, A
J	Current efficiency, %
J_p	Current density, A/cm^2
T	Temperature, K
t	Time, s
V	Volume, m^3
DC	Direct current
e^-	Electron
ICP-OES	Inductively Coupled Plasma Optical Emission Spectrometer
RHE	Reversible hydrogen electrode
H_2	Hydrogen gas
H_2O	Water
H_3BO_3	Boric acid
HCl	Hydrochloric acid
KCl	Potassium chloride
NaCl	Sodium chloride
NH_4Cl	Ammonium chloride
NiOOH	Nickel (III) oxide
O_2	Oxygen gas
PbO_2	Lead (II) oxide
RuO_2	Ruthenium (IV) oxide
Zn	Zinc
$ZnCl_2$	Zinc chloride

LIST OF APPENDICES

CHAPTER 1

INTRODUCTION

1.1 Background

Heavy metals are categorized as elements with density higher than 5 g/cm^3 (Barakat, 2011). Industrial wastewaters containing heavy metals are discharged by industries such as mining industry, metal plating industry, battery production industry, fertilizer industry, etc (Fu and Wang, 2010). The commonly found heavy metals in industrial wastewater are lead, chromium, copper, nickel, cobalt, mercury, cadmium and zinc. Heavy metals are non-biodegradable and can accumulate in living organisms, causing a number of health disorders.

Zinc is one of the heavy metals found in wastewater discharged from galvanizing and alloy industries (Liu et al., 2014). Zinc is a transition metal element with atomic number 30 and atomic weight 65.38 g/mol. It exists in solid state at room temperature, normally in +2 oxidation state. The melting point of zinc is 692.68 K, boiling point is 1180 K and density is 7.14 g/cm^3.

Zinc is widely applied in galvanizing steel or iron for corrosion protection and as an alloying element for brass and copper. In galvanization, zinc acts as a sacrificial anode by forming a thin surface film of zinc “patina” to protect the steel against corrosion. Other application includes zinc-base die castings, where it has less die wear and better surface finishes due to its lower melting point compared to magnesium and aluminum die castings (Campbell, 2008). Zinc and its alloys are also

applied in electrical components, hardware and automotive sectors. These industries are the main contributors to zinc-containing wastewater.

Zinc wastes can enter human body through intake of drinking water or meats containing zinc. Zinc poses acute toxicity to human health but it does not cause any known chronic effects (Sullivan and Krieger, 2001). The toxic effects of zinc include depression, neurological upsets, lethargy and increased thirst. The maximum contaminant level (MCL) standard for zinc is 0.80 mg/L (Barakat, 2011). Whereas, the U.S. Environmental Protection Agency recommends zinc concentration in drinking water to be less than 5 ppm (Agency for Toxic Substances & Disease Registry, 2005).

The long term solutions to prevent and/or reduce the discharge of heavy metals into environment are source reduction and waste minimization (Lewinsky, 2007). However, downstream wastewater treatment technologies are also important to control the discharge concentration of zinc. The presently applied wastewater treatment technologies include ion exchange, membrane filtration, chemical precipitation, adsorption, electrochemical treatment, etc.

Electrochemical method is a promising wastewater treatment technology that has gained considerable attentions in the past two decades, including electrocoagulation, electroflotation, electrooxidation, electrodisinfection and electrodeposition processes. This method offers a wide range of competitive advantages compared to other technologies, such as high removal efficiency, clean energy conversion, easy operation and low environmental impact (Mook, Aroua and Issabayeva, 2014). In addition, it is a versatile and benign technology that can be applied in different wastewater treatment because the main reagent is electron (Ghanbari and Moradi, 2014).

Various researches have been carried out to study the removal of zinc from industrial wastewater. Mansoorian, Mahvi and Jafari (2014) conducted electrocoagulation process to remove zinc from battery industry wastewater. They successfully removed 95.2% of zinc using iron electrode at 6 mA/cm^2 current density and 93.3% using stainless steel electrode at 8 mA/cm^2 current density, by using

alternating current. In addition, Paduraru et al. (2014) discovered that rapeseed waste was an effective biosorbent for zinc removal at 39 % to 89 % efficiency. Micellar-enhanced ultrafiltration of zinc using spiral-wound membrane also showed promising results (Rahmanian, Pakizeh and Maskooki, 2010).

However, the fate of zinc removed from wastewater stream is questionable: should the treatment media saturated with zinc be disposed of, or should it be put into a useable form, e.g. recovered as metallic solid. Disposal of treatment media is definitely the cheapest option, notwithstanding the diminishing landfills available and leaching of zinc into groundwater via all possible routes. An alternative option is to recover zinc waste by electrodeposition onto a cathode material, which is an effective electrochemical method to recover heavy metals from wastewater stream (Chen, 2003). Recovery of metallic zinc from wastewater stream can offset the increasing purchase cost of raw zinc, at the same time reducing exploitation from natural resources which certainly comes with significant impacts on the environment.

Electrodeposition requires the investment of electrical power as the energy source. In the scenario where the energy invested for recovery is much greater than the energy invested to mine from natural resources, this option is not economically feasible. Hence, the parameters optimization for zinc recovery by electrodeposition at the minimized energy input is an important topic of research nowadays.

To recover zinc from wastewater by electrodeposition, it is important to select the right type of electrolyte that favors zinc deposition, which is the core of the recovery process. Other parameters such as electrode materials, electrolyte temperature, electrolyte pH and electrolysis current have equal significance to optimize the recovery process. Skoog et al. (2004) reported that current density, temperature and additives are the principal factors that influence the physical characteristics of metallic deposits.

In this research project, the application of electrochemical methods to recover zinc from aqueous solution obtained through wastewater treatment: desorption and recovery of zinc, are thoroughly studied. Resource recovery means that the materials

are removed from the waste stream and be purchased by an end user (Masters and Ela, 2008). Hence, this research also studies the feasibility of zinc recovery.

1.2 Aims and Objectives

This research project aims to desorb zinc from activated carbon and recovered as metallic zinc with high purity via electrochemical method. The objectives of the research include:

i. To desorb zinc ions from palm shell activated carbon surface.
ii. To apply electrochemical method to recover zinc from aqueous solution.
iii. To determine the efficiency of zinc recovery.

CHAPTER 2

LITERATURE REVIEW

2.1 Zinc Electrodeposition

Electrodeposition refers to the formation of a metallic coating on a base material by electrochemical reduction of the metallic ions from an electrolyte (Gamburg and Zangari, 2011). This process occurs when an external power supplies electrical current to the electrolyte via two electrodes. As a result, the metallic cations are reduced and deposit onto the cathode connected to the negative terminal of the external power. On the other hand, the anode dissolves into the electrolyte as anion if it is a reactive electrode, or anions from the electrolyte are selectively discharged at the anode if it is an inert electrode, connected to the positive terminal of the external power. Electrons are donated by the oxidized anions, transfer across the external electrical circuit and accepted by the reduced cations.

The main application of zinc electrodeposition is to galvanize steel substrates for corrosion protection and aesthetic value in automotive, construction, electrical, appliances and material industries. During electrodeposition, Zn^{2+} ions from the electrolyte are reduced to metallic zinc which deposits onto the cathode material. Hydrogen evolution is the competing electrochemical reaction. The possible cathodic half-reactions are (Skoog et al., 2004):

$$2H^+ + 2e^- \leftrightarrow H_2(g) \qquad E_0 = 0.000\ V \qquad (2.1)$$

$$Zn^{2+} + 2e^- \leftrightarrow Zn(s) \qquad E_0 = -0.763\ V \qquad (2.2)$$

Water electrolysis happens at the anode where water molecule splits into H^+ ion and O_2 gas. Other side reactions such as dissolution of the reactive anode or oxidation of competing anions can occur, depending on the type of electrolyte used. The possible anodic half-reaction is (Skoog et al., 2004):

$$O_2(g) + 4H^+ + 4e^- \leftrightarrow 2H_2O \qquad E_0 = 1.229\ V \tag{2.3}$$

2.2 Adsorption and Desorption of Zinc

Activated carbon refers to amorphous carbonaceous material that is characterised by high porosity and large inter-particulate surface area. It is also known as an efficient adsorbent for heavy metals due to its large surface area and chemical properties which depend on the raw carbon source and activation method. Adsorption of metallic cations takes place due to electrostatic attraction with the negatively-charged sites on activated carbon surface produced by ionization of its surface acidic groups. Adsorption greatly depends on the solution pH; it increases with increasing surface acidity of the carbon surface (Bansal and Goyal, 2005).

Zinc removal from wastewater stream can be achieved by adsorption onto activated carbon. Gonzalez and Pliego-Cuervo (2014) performed adsorption batch studies using mesoporous activated carbon produced from *Bambusa vulgaris striata* to remove zinc ions in aqueous solution. The results indicated more than 98 % removal efficiency of Zn^{2+} ions. This studies suggested 0.6 g/L dose of activated carbon, solution at pH 9 and 16 hours of equilibrium time in static conditions. In addition, Rao et al. (2007) demonstrated that activated carbon prepared from *Ceiba pentandra* hulls successfully removed 99.1 % zinc using 10 g/L sorbent in batch test experiment. The optimum conditions were solution at pH 6 and 50 minutes of equilibrium time. These findings prove that zinc removal by adsorption onto activated carbon can accomplish removal efficiency as high as 98 %.

Zn^{2+} ions adsorbed onto activated carbon can be desorbed using hydrochloric acid, by the chemical equation:

$$Zn^{2+} + 2HCl \rightarrow ZnCl_2 + H_2 \quad (2.4)$$

Since 1 mol of HCl desorbs 1 mol of Zn^{2+} ion, the theoretical concentration of desorbed Zn^{2+} ion could be estimated by the concentration of HCl used. Desorption takes place when the coordination of metallic ions with activated carbon is disrupted, causing the release of these metallic ions from the activated carbon surface. Rao et al. (2007) performed desorption studies using HCl in the range of 0.05 to 0.25 M concentration. Desorption increased with increasing concentration of HCl, but remained constant beyond 0.15 M HCl. The studies showed that 0.15 M HCl attained 70 % desorption efficiency for zinc.

In this research project, the desorption product is zinc chloride. This desorption product provides the Zn^{2+} ions in aqueous solution for subsequent recovery by electrochemical method.

2.3 Electrolyte Constituents for Zinc Electrodeposition

Acid chloride bath comprises of two major types, which are ammonium chloride bath and potassium chloride bath. Sodium chloride bath is also a type of acid chloride bath (Winand, 2010) but it is rarely found in literature.

Four agents make up an acid chloride bath. The first agent is zinc anode or zinc chloride that provides Zn^{2+} ions for electrodeposition. The second agent is conductivity salt that improves the electrical conductivity of electrolyte, such as ammonium chloride, potassium chloride or sodium chloride. The third agent is buffering agent which maintains the pH of the bath, in which boric acid is commonly used. During elecrodeposition, hydrogen evolution at the cathode consumes H^+ ions from the electrolyte that is released as H_2 gas. This leads to higher pH near the electrode surface. The presence of buffering agent prevents precipitation of metal hydroxide due to the increase in pH near the electrode surface (Gamburg and Zangari, 2011). The forth agent is additive which can be a brightener, leveling agent, wetting

agent and/or grain refiner. Some additives have a combination of any of the above four functions, for example, an additive which is both a brighter and a grain refiner.

Winand (2010) suggested using acid chloride baths that are either all ammonium chloride, low ammonium or all potassium chloride. The electrolyte baths can be a combination of ammonium chloride with potassium chloride, or with sodium chloride, but not a combination of potassium chloride with sodium chloride. Boric acid is only used in potassium chloride bath. Moreover, higher concentration of potassium chloride is required as the conductivity salt compared to ammonium chloride, probably because potassium chloride is a weaker conductivity salt. Sodium chloride is rarely used due to its lower cathode efficiency and higher corrosion rate to the electrode than potassium chloride (Loto, 2012). The bath constituents and compositions of acid chloride bath are listed in Table 2.1.

Table 2.1: Composition of Acid Chloride Baths (g/L)

Constituent	**All Ammonium Chloride**	**Low Ammonium**		**All Potassium Chloride**
		Potassium Chloride	**Sodium Chloride**	
Zn	15 – 30	15 – 30	15 – 30	22 – 38
NH_4Cl	120 – 180	30 – 45	30 – 45	–
KCl	–	120 – 150	–	185 – 225
NaCl	–	–	120	–
Boric acid	–	–	–	22 – 38
Carrier brightener	4 vol%	4 vol%	4 vol%	4 vol%
Primary brightener	0.25 %	0.25 %	0.25 %	0.25 %

(Winand, 2010. p. 290)

Similarly, Porter (1991) did not recommend boric acid in an ammonium chloride bath, and potassium chloride is needed at higher concentration than ammonium chloride. Table 2.2 shows the composition and concentration of electrolyte constituents in ammonium chloride and potassium chloride bath.

Table 2.2: Composition of Acid Chloride Baths and Characteristics

Bath and Composition	Concentration (g/L)	Characteristics
Ammonium chloride bath		
$ZnCl_2$	15 – 60	Dull deposit without
NH_4Cl	180 – 225	brighteners.
Zinc	30 – 75	
Chloride and brighteners	120 – 150	
Potassium chloride bath		
$ZnCl_2$	73	Not available
KCl	210 – 240	
Boric acid and brighteners	25	

(Porter, 1991. p. 271)

Yu et al. (2013) conducted zinc electrodeposition using potassium chloride bath that contained boric acid. Benzylideneacetone and sodium benzoate were added to the electrolyte solution as additives to improve the surface morphology and crystallinity of zinc deposit. The composition of zinc coatings electrodeposition solution used by Yu et al. is listed in Table 2.3.

Table 2.3: Composition of Zinc Coatings Electrodeposition Solution

Constituent	Concentration (M)
$ZnCl_2$	0.2
KCl	2.0
Boric acid	0.5
Benzylideneacetone	0.1
Sodium Benzoate	0.5

(Yu et al., 2013. p. 235)

In contrast, Saber, Koch and Fedkiw (2002) recommended boric acid in ammonium chloride bath. The additives used were different from Yu et al., which were polyacrylamide and thiourea. Table 2.4 shows the composition of zinc chloride plating bath at pH 4.7.

Table 2.4: Composition of Zinc Chloride Plating Bath at pH 4.7

Constituents	Concentration
$ZnCl_2$	0.4 M
NH_4Cl	2.2 M
Boric acid	0.35 M
Polyacrylamide	0.2 – 1.5 g/L
Thiourea	0.02 – 0.5 g/L

(Saber, Koch and Fedkiw, 2002. p. 175)

Potassium chloride and ammonium chloride are also known as supporting electrolyte. They are non-reactive and will not react at the electrode (Skoog et al., 2004). On the other hand, hydrogen evolution is favored at cathodic potential due to its more positive reversible potential; therefore it is not possible to deposit zinc. However, Zhang (1996) reported that by increasing zinc concentration above 10^{-4} M (6.5409×10^{-3} g/L), the cathodic reaction will be dominated by zinc deposition.

In potassium chloride bath, KCl serves as conductivity salt and weak ligands of Zn^{2+} ions. The concentration of Cl^- ions should be kept higher than Zn^{2+} ions to form the high coordination complex $K_4(ZnCl_6)$ to increase cathodic polarization and improve throwing power (Yu et al., 2013). On the other hand, NH_4Cl serves as conductivity salt in ammonium chloride bath. Ammonium chloride bath can be operated at high current density but it requires expensive chlorination of the disposed bath (Winand, 2010).

Boric acid acts as buffering agent to maintain the pH of electrolyte where at equilibrium:

$$H_3BO_3 + 3H_2O \leftrightarrow 3H_3O^+ + (BO_3)^{3-} \quad (2.5)$$

As H^+ ions are removed as H_2 gas, the equilibrium shifts to the right and boric acid dissociates to balance the concentration of H^+ ions in the electrolyte.

2.4 Electrode Materials

An active electrode takes part in the electrochemical reaction, either by anodic dissolution or cathodic deposition. A passive electrode does not take part in the electrochemical reaction. Its function is to complete the electrical circuit by donating or accepting electrons, without anodic dissolution or cathodic deposition (Jensen, 2009). This research project requires an active cathode and a passive anode. It is desirable to select electrode material that enhances the overpotential for hydrogen evolution and hence reduces the cathodic side reaction. The characteristics of different electrode materials, their advantages and disadvantages are reviewed in this section.

Stainless steel contains carbon, nickel, manganese and chromium. Stainless steel electrode is the cheapest electrode for weakly alkaline or nearly neutral aqueous electrolytes, with more than –200 mV versus Reversible Hydrogen Electrode (RHE) hydrogen overpotential. Lead or cadmium coatings can provide high overpotential for hydrogen evolution. However, chromium in stainless steel can slowly dissolve into the electrolyte forming the toxic hexavalent chromium. Stainless steel is passivated in weakly alkaline or phosphate electrolytes, hence it is suitable as oxygen evolving anode to prevent oxygen evolution (Wendt and Kreysa, 1999).

Mild steel contains carbon, copper, manganese and silicon. It is cheap but not as efficient as stainless steel electrode, because regular surface cleaning during electrolysis is required to remove the surface rust which may inhibit the desired deposition.

Nickel electrode is more expensive than steel electrode and it is used only when electrode passivity is required. However, nickel electrode is not passivated in strong acidic electrolytes or alkaline electrolytes containing complex forming agents. For example, nickel oxyhydroxide NiOOH is formed on the electrode surface before oxygen evolution in alkaline electrolyte (Wendt and Kreysa, 1999).

Lead electrode is suitable as oxygen evolving anode because it is passivated by the formation of lead dioxide in strongly acidic aqueous electrolytes, for example unalloyed Pb/PbO_2 anode. To reduce the overpotential for oxygen evolution, silver is alloyed onto lead electrode (Wendt and Kreysa, 1999).

Titanium electrode is stable against surface and pitting corrosion in acidic and slightly basic aqueous solution. To reduce the overpotential for anodic chlorine and oxygen evolution, titanium electrode is coated with RuO_2, metal oxides or metals of the platinum group. However, it is not suitable as cathode due to embrittlement caused by hydrogen evolution (Wendt and Kreysa, 1999).

Platinum is expensive to be used as a bulk electrode. It is normally coated onto the surface of a support electrode such as carbon electrodes. Platinum electrode is corrosion resistance, inert and does not dissolve in electrolyte. Also, graphite electrode is corrosion resistant, inert and does not dissolve in electrolyte.

Skoog et al. (2004) claimed that the overpontential of hydrogen is high on copper, lead and mercury electrodes, thus zinc can be deposited on these electrodes with insignificant amount of hydrogen evolution. Naik, Venkatesha and Nayak (2011) and Saber, Koch and Fedkiw (2002) used zinc anode in order to provide Zn^{2+} ions to the electrolyte solution by electrochemical dissolution. Yu et al. (2013) suggested platinum as the anode but this electrode material is very costly. Mild steel, low carbon steel and iron are recommended too but these electrode materials have the tendency to corrode in acid chloride baths. Table 2.5 lists the electrode materials and their dimensions used in different studies.

Table 2.5: Electrode Materials and Dimensions Reported by Literatures

Bath	Anode	Cathode	Dimensions	Literatures
Potassium chloride	Mild steel	Mild steel	10 cm long 1 cm wide	Loto and Loto (2013)
Ammonium chloride	Zinc plate	Mild steel	2.4×10 cm^2	Naik, Venkatesha and Nayak (2011)
Ammonium chloride	Zinc sheet	Low carbon steel	0.317 cm^2 surface area 0.1 cm thickness	Saber, Koch and Fedkiw (2002)
Potassium chloride	Platinum	Iron	0.2×0.2 dm^2	Yu et al. (2013)

In this research project, stainless steel electrode is selected as the cathode to resist corrosion in acid chloride bath. A corrosion resistant electrode can prevent the dissolution of electrode material into the electrolyte, which could contaminate the bath and adversely affect the results. Graphite electrode is selected as the anode due to its chemical inertness.

2.5 Electrolyte Temperature

Generally, high temperature can increase the solubility of metallic salt in the electrolyte and its electrical conductivity, while decreasing the tendency for anodic passivation. However, high temperature can also enhance the evaporation of electrolyte and corrosion of electrodes. On the other hand, low temperature requires lower current density to prevent electrodeposition under diffusion limiting conditions. Also, low temperature often forms stressed deposits that are prone to embrittlement due to slower diffusion kinetics (Gamburg and Zangari, 2011). Temperature effects

on the deposition rate, current efficiency, crystalline structure and surface morphology are discussed in the following subsections.

2.5.1 Effects of Temperature on Deposition Rate

Yu et al. (2013) varied the bath temperature from 293 to 333 K in a chloride zinc system for 1800 s, at pH 5 and current density 4 A/dm^2 using platinum anode and iron cathode. As shown in Figure 2.1, the deposition rate increased from 170 to 226 mg/h when temperature increased from 293 to 333 K. At higher temperature, bath viscosity decreases which causes bath conductivity to increase. As a result, mass transfer rate of ions and subsequently deposition rate also increase.

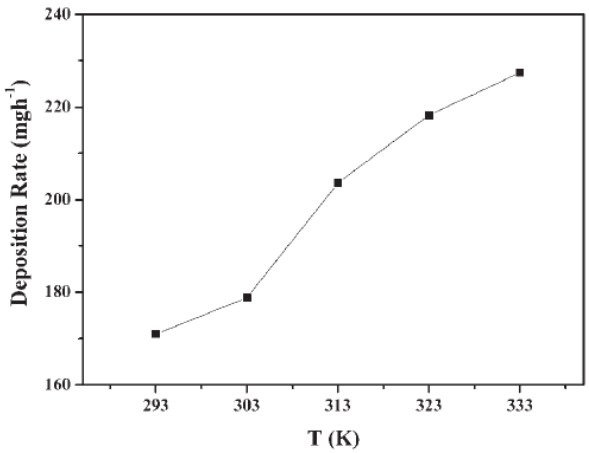

Figure 2.1: Effects of Temperature (K) on Deposition Rate (mg/h) (Yu et al., 2013. p. 235)

2.5.2 Effects of Temperature on Current Efficiency

At higher temperature, current efficiency also increases due to an increase in bath conductivity and mass transfer rate of ions. As shown in Figure 2.2, current efficiency increased from 70 to 95% when temperature increased from 293 to 333 K.

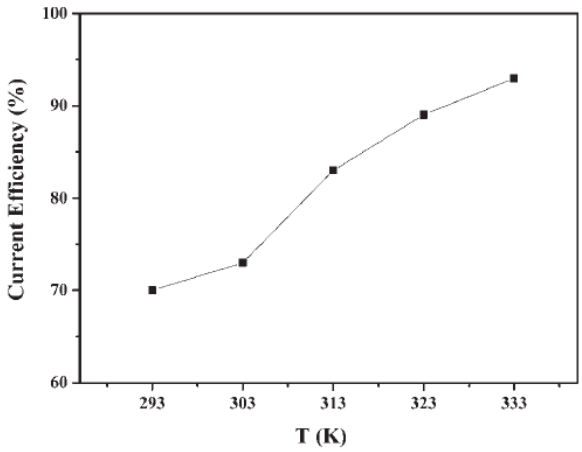

Figure 2.2: Effects of Temperature (K) on Current Efficiency (%) (Yu et al., 2013. p. 236)

2.5.3 Effects of Temperature on Crystalline Structure and Surface Morphology

Figure 2.3 shows the X-ray diffraction patterns of zinc deposits with its characteristic peaks at different temperatures. The peak intensity decreased when temperature increased. This infers that the crystallinity of zinc decreases at higher temperature due to thermal decomposition of refiner additives.

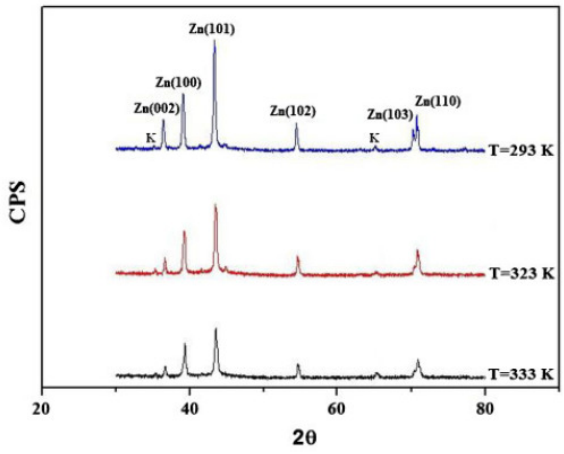

Figure 2.3: X-ray Diffraction Patterns of Zinc Deposits at Different Temperatures (Yu et al., 2013. p. 236)

Figure 2.4 shows the surface morphology of zinc deposits at 293, 323 and 333 K obtained by atomic force microscopy. Zinc deposit had larger bulk structure at 293 K while smaller bulk structure was observed at 323 K. At 333 K, mountainous structure with rough surface was obtained due to thermal decomposition of refiner additives.

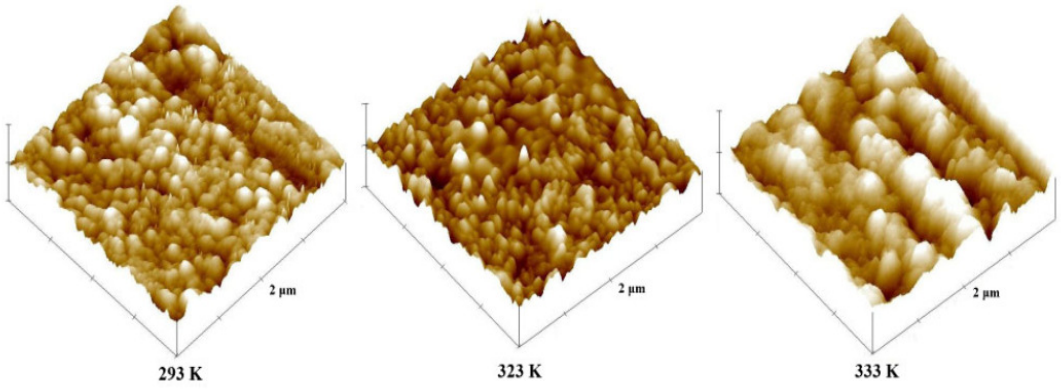

Figure 2.4: Zinc Deposits at 293, 323 and 333 K by Atomic Force Microscopy (Yu et al., 2013. p. 237)

The mentioned findings suggest that the optimum bath temperature is 323 K due to increased bath conductivity, mass transfer rate of ions and current efficiency. Although the crystalline structure is not the optimum, the surface morphology is fine-grained which is desirable. Table 2.6 lists the operating temperature used in different studies.

Table 2.6: Operating Temperature (K) Reported by Literatures

Bath	Temperature (K)	Literatures
Ammonium chloride	288 – 313	Gamburg and Zangari (2011)
Aluminum chloride	298 – 308	
Ammonium chloride	296±1	Saber, Koch and Fedkiw (2002)
Ammonium chloride	294 – 300	Zhang (1996)
Ammonium chloride	298	

Table 2.6 shows that the operating temperature falls in the range of 288 to 313 K. In acid chloride bath, low temperature can lead to whitish zinc deposits, precipitation and crystallization of the bath constituents. The precipitates can clog the system and increase the roughness of deposit. On the other hand, high temperature can adversely affect the luster of deposit and bath stability (Brankovic and Rajeshwar, 2008).

2.6 Electrolyte pH

High pH levels can cause precipitation of the bath constituents and polarization of anode (Brankovic and Rajeshwar, 2008). Acid chloride bath operates in the acidic pH range. Table 2.7 lists the pH used in different studies.

Table 2.7: pH of Acid Chloride Bath Reported by Literatures

Bath	pH	Literature
Ammonium chloride	4.5 – 6.0	Gamburg and Zangari (2011)
Aluminum chloride	3.5 – 4.5	
Ammonium chloride	4.5	Naik, Venkatesha and Nayak (2011)
Ammonium chloride	4.7	Saber, Koch and Fedkiw (2002)
Ammonium chloride	5.2 – 6.2	Zhang (1996)
Potassium chloride	5	Yu et al. (2013)

Ammonium chloride bath operates in the pH range of 4.5 to 6.2, while potassium chloride bath operates at pH 5. Aluminum chloride bath is rarely used, hence it is not reviewed.

2.7 Electrolysis Current

Pulse electrodeposition can produce a harder, purer deposit (Porter, 1991). Pulse electrodeposition can also produce finer grained deposit by favouring the initiation of grain nuclei and increases the number of grains per unit area (Zemanova & Cocural, 2010). Pulse electrodeposition utilizes a pulsed DC rectifier as the current source. The current is alternated between an ON-time and an OFF-time. Electrodeposition occurs when the current source is switched on for a short period. Electrodeposition stops with some loss of the coating when the current source is switched off for a short period. The three parameters that influence the deposit properties in pulse electrodeposition are peak current density, current ON-time and current OFF-time (Saber, Koch and Fedkiw, 2002).

Saber, Koch and Fedkiw (2002) varied the pulse peak current density J_p from 0.4 to 2 A/cm^2, at 0.1 ms current-ON time and 1 ms current-OFF time, in an ammonium chloride bath. Figure 2.5 shows the SEM images of zinc deposits at different J_p's, with polyacrylamide and thiourea as additives. At 0.4 A/cm^2, the zinc deposit was characterized with large grain size of 4 – 5 µm. The grain size decreased to 1 – 1.5 µm when J_p increased from 0.8 to 1.6 A/cm^2.

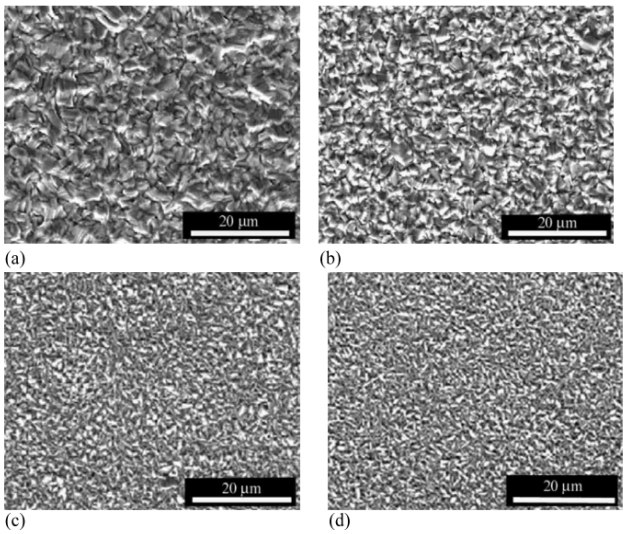

Figure 2.5: SEM images of zinc deposit with additives at J_p (a) 0.4 A/cm^2 (b) 0.8 A/cm^2 (c) 1.2 A/cm^2 (d) 1.6 A/cm^2 (Saber, Koch and Fedkiw, 2002. p. 176)

Next, Figure 2.6 shows the SEM images of zinc deposit at different J_p's, without additives. The grain size decreased when J_p increased, where the smallest grain size of 4 – 5 µm was obtained at 2 A/cm^2.

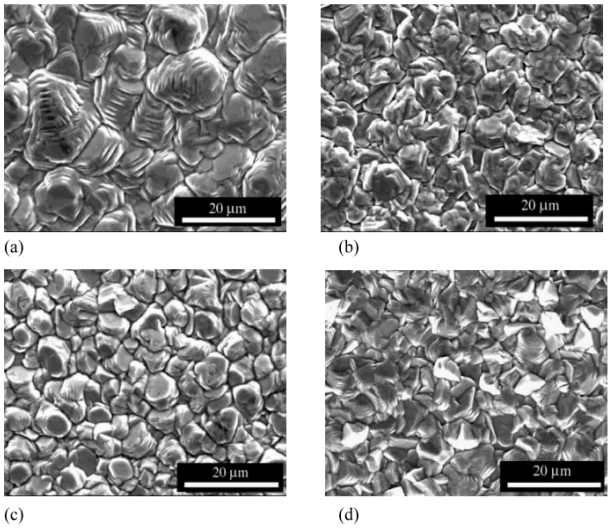

Figure 2.6: SEM images of zinc deposit without additives at J_p (a) 0.4 A/cm^2 (b) 0.8 A/cm^2 (c) 1.6 A/cm^2 (d) 2 A/cm^2 (Saber, Koch and Fedkiw, 2002. p. 178)

Saber, Koch and Fedkiw (2002) suggested that high J_p increases the overpotential and free energy to form new nuclei, resulting in higher nucleation rate and smaller grain size. Hence, pulse electrodeposition technique at 2 A/cm^2 peak current density, combined with additives, can produce nanocrystalline zinc deposit. Nonetheless, Skoog et al. (2004) claimed that the best deposits are formed at less than 0.1 A/cm^2. Table 2.8 lists the current density used in different literatures.

Table 2.8: Current density of acid chloride bath reported by literatures

Bath	Current Density	Literatures
Ammonium chloride	5 – 40 A/cm^2	Gamburg and Zangari (2011)
Aluminum chloride	15 – 70 A/cm^2	
Ammonium chloride	0.4 – 2 A/cm^2 pulsed DC	Saber, Koch and Fedkiw (2002)
Ammonium chloride	0.3 – 5 A/dm^2	Zhang (1996)
Ammonium chloride	1 A cell current	

CHAPTER 3

METHODOLOGY

3.1 Procedures of Zinc Adsorption

500 mL of synthetic zinc solution was prepared by dissolving 0.1137 g of zinc nitrate hexahydrate $Zn(NO_3)_2 \cdot 6H_2O$ (Systerm, ChemPur) and 6.4743 g of sodium nitrate $NaNO_3$ (R&M, Chemicals) solids in de-ionized water to obtain 50 ppm Zn^{2+} ions and 0.15 M $NaNO_3$. 1 ppm is equivalent to 1 mg/L. Then, 10 g of palm shell activated carbon with 8 × 30 mesh size and > 1000 iodine number was immersed in synthetic zinc solution for 24 hours to adsorb Zn^{2+} ions into activated carbon. After 24 hours of batch adsorption, the solution was filtered and analyzed by Inductively Coupled Plasma Optical Emission Spectrometer ICP-OES (Optima 7000 DV, Perkin Elmer) to determine the concentration of Zn^{2+} ions remained in the solution. The concentration of Zn^{2+} ions adsorbed into activated carbon was computed by equation 3.1.

$$C_{adsorbed} = C_{before\ adsorption} - C_{after\ adsorption} \tag{3.1}$$

where

C_{adsorbed} = Concentration of Zn^{2+} ions adsorbed into activated carbon, ppm

$C_{\text{before adsoption}}$ = Concentration of Zn^{2+} ions in synthetic zinc solution before adsorption, ppm

$C_{\text{after adsoprtion}}$ = Concentration of Zn^{2+} ions in solution after adsorption, ppm

3.2 Procedures of Zinc Desorption

After 24 hours of batch adsorption, the activated carbon was immersed in 500 mL of 10 % HCl (Fisher Scientific) for another 24 hours to desorb Zn^{2+} ions out from activated carbon. After 24 hours of batch desorption, the solution was filtered and analyzed by ICP-OES to determine the concentration of Zn^{2+} ions desorbed out from activated carbon. The desorption efficiency of Zn^{2+} ions by 10 % HCl was computed by equation 3.2.

$$Desorption\ efficiency = \frac{C_{adsorbed} - C_{desorbed}}{C_{adsorbed}} \times 100\ \% \qquad (3.2)$$

where

$C_{adsorbed}$ = Concentration of Zn^{2+} ions adsorbed into activated carbon, ppm

$C_{desorbed}$ = Concentration of Zn^{2+} ions in solution after desorption, ppm

3.3 Preparation of Electrolyte Solutions

The solution after batch desorption consisted of zinc chloride. Four types of electrolyte solution of 250 mL were prepared. The first type was control electrolyte which consisted of only $ZnCl_2$. Three solutions of the first type were prepared to test for three variables, which were control electrolyte, electrolyte temperature and pulse current. The second type was potassium chloride electrolyte that consisted of $ZnCl_2$ and 1.0 M KCl (Systerm, ChemAR) which acted as the conductivity salt. The third type was buffer electrolyte that consisted of $ZnCl_2$ and 0.5 M boric acid (R&M, Chemicals) which acted as pH buffer. The forth type was electrolyte at pH 4.5 that consisted of $ZnCl_2$ and sodium hydroxide (R&M, Chemicals) which raised the electrolyte pH to 4.5. The compositions of each constituent were varied by dilution equation (3.3).

$$C_1V_1 = C_2V_2 \quad (3.3)$$

where

C_1 = Concentration before dilution, M
V_1 = Volume before dilution, mL
C_2 = Concentration after dilution, M
V_2 = Volume after dilution, mL

3.4 Experimental Setup

The experimental setup consisted of Potentiostat/Galvanostat/ZRA (Gamry Instruments, Reference 600), stainless steel electrode, graphite electrode, silver/silver chloride electrode, hot plate (Corning, PC-620D), pH meter (Trans Instruments), 500 mL beaker and 250 mL electrolyte solution. The experimental setup is shown in Figure 3.1.

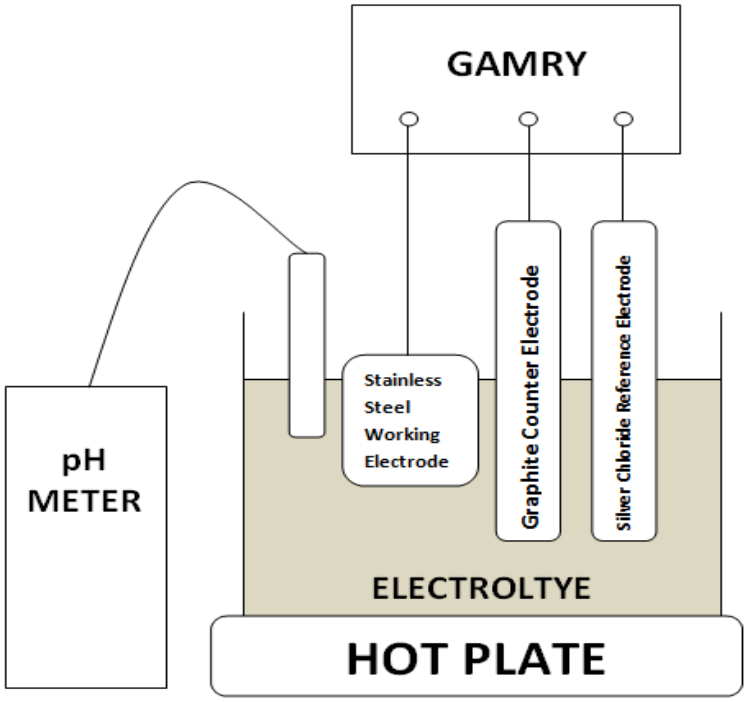

Figure 3.1: Experimental setup

A three-electrode system was used, in which stainless steel electrode was used as the working electrode, graphite electrode as the counter electrode and Ag/AgCl electrode as the reference electrode. The stainless steel electrode was plate-shape with the dimension of 4 cm width, 4 cm length and 0.1 cm thickness. The graphite electrode and Ag/AgCl electrode were rod-shape. The three electrodes were placed close together to minimize electrical resistance in the electrolyte solution between the electrodes. 250 mL electrolyte solution was contained in a 500 mL beaker. The electrolyte temperature was controlled by the hot plate. The electrolyte pH was monitored by the pH meter.

3.5 Cyclic Voltammetry Procedure

First, the stainless electrode was polished with abrasive paper, degreased by wiping with isopropyl alcohol, rinsed with distilled water, activated in 20 % sulphuric acid bath for 30 seconds, rinsed with distilled water again and blown dry (Zemanova and Cocural, 2010). The graphite electrode and Ag/AgCl electrode were rinsed with distilled water to remove surface impurities.

Next, 250 mL of synthetic zinc solution containing 50 ppm Zn^{2+} ions and 0.15 M $NaNO_3$ was subjected to cyclic voltammetry. The experimental setup was manipulated in Gamry Framework. Scan limit 1 was set at 1.3 V while scan limit 2 was set at –1.3 V, versus the Ag/AgCl reference electrode. The electrode area was set at default value of 1 cm^2 which signified the user did not wish to enter the electrode area. Other parameters were set at their respective default values. A cyclic voltammogram was generated in Gamry Echem Analyst, in which the reduction of Zn^{2+} ions to zinc deposit was determined from the cathodic peak potential E_{pc}. The experimental setup of cylic voltammetry in Gamry Framework is shown in Figure 3.2.

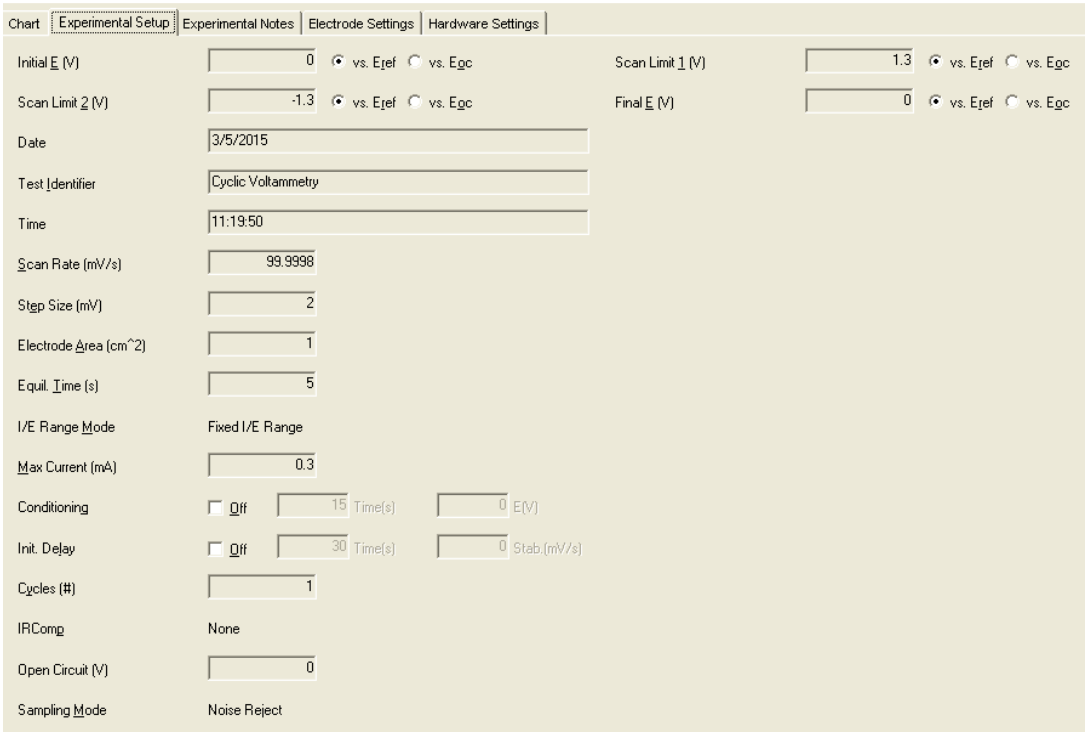

Figure 3.2: Experimental setup of cyclic voltammetry in Gamry Framework

3.6 Procedures of Zinc Electrodeposition

Six tests were carried out to study the effects of six variables on zinc electrodeposition. These variables were control electrolyte, conductivity salt, pH buffer, electrolyte temperature, electrolyte pH and pulse current. The first test was control electrolyte without manipulation of other variables. The second test studied the effect of KCl as the conductivity salt. The third test studied the effect of boric acid as the pH buffer. The forth test studied the effect of bath temperature at 45 ^{o}C. The fifth test studied the effect of pH at pH 5.

The first five tests were subjected to chronoamperometry for 60 minutes duration. The experimental setup was manipulated in Gamry Framework. The step 1 voltage was set at +1.297 V, as determined from the cathodic peak potential of cyclic voltammogram in section 3.5, while the step 2 voltage was set at 0 V, versus the Ag/AgCl reference electrode. The step 1 time was set at 3600 s (1 hour) while the step 2 time was set at 0 s. The electrode area was set at default value of 1 cm^2 which

signified the user did not wish to enter the electrode area. Other parameters were set at their respective default values. The experimental setup of chronoamperometry in Gamry Framework is shown in Figure 3.3.

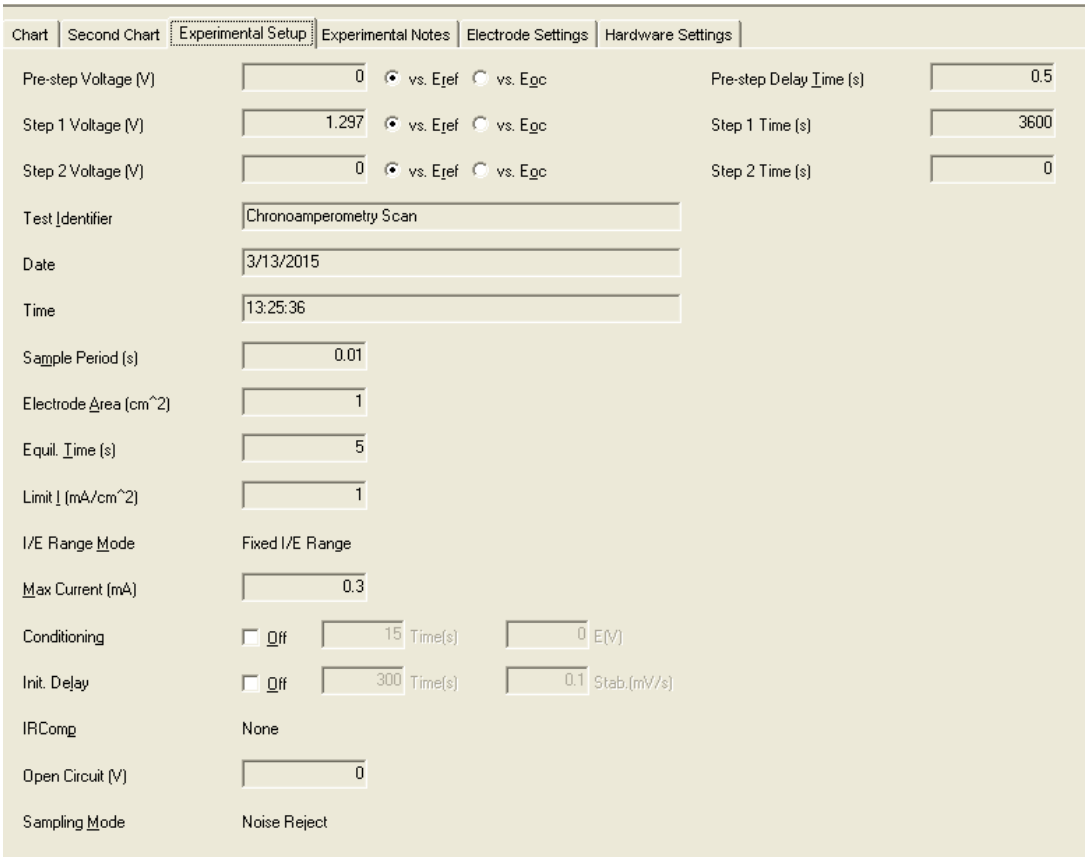

Figure 3.3: Experimental setup of chronoamperometry in Gamry Framework

Lastly, the sixth test studied the effect of pulse current subjected to repeating chronoamperometry for 40 minutes duration. The experimental setup was similar to chronoamperometry, with the exception of step 1 time being set at 5 s and step 2 time at 5 s. This produced a pulse current in which the potential was stepped up to +1.297 V for 5 s and then stepped down to 0 V for 5 s, and the cycle continued for 40 minutes. The experimental setup of repeating chronoamperometry in Gamry Framework is shown in Figure 3.4.

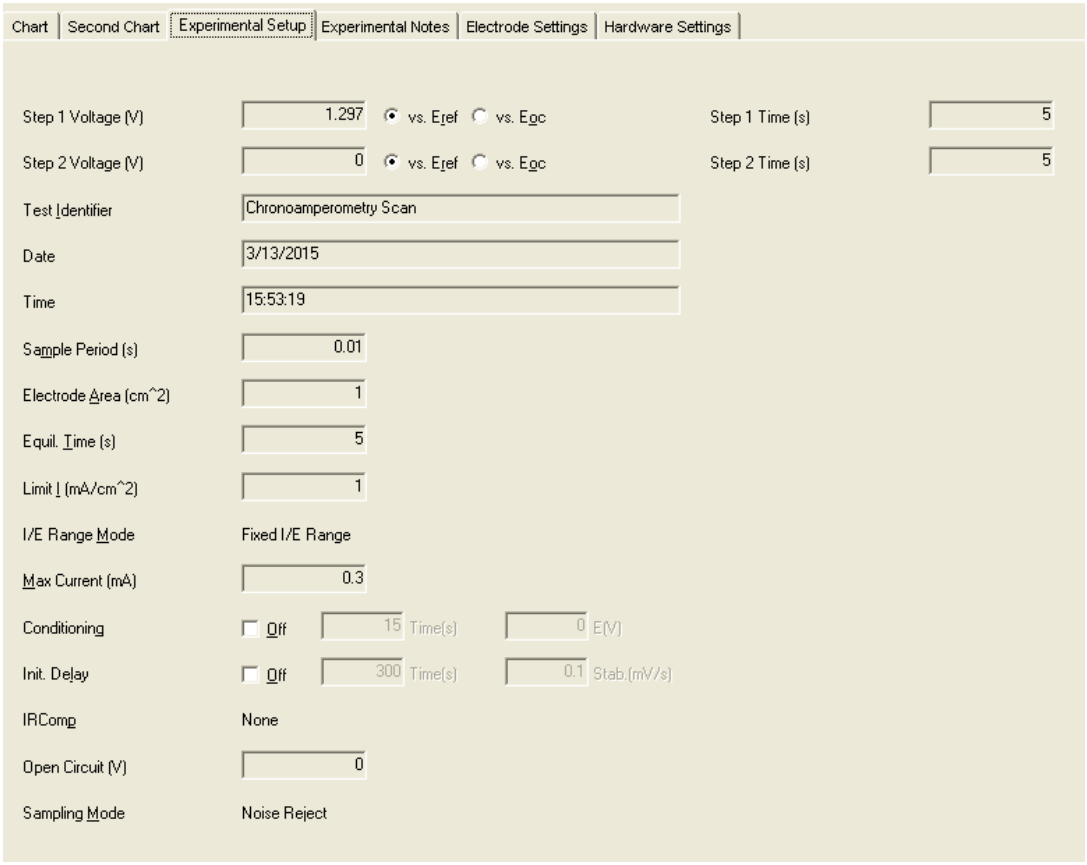

Figure 3.4: Experimental setup of repeating chronoamperometry in Gamry Framework

3 mL samples of electrolyte solution were taken and electrolyte pH was measured at 5 minutes interval. 13 samples of electrolyte solution were taken for chronoamperometry experiment while 9 samples of electrolyte solution were taken for repeating chronoamperometry experiment for ICP-OES measurement of zinc concentration. Chronoamperometry scan of voltage (mV) and current (μA) versus time (ks) for each test was generated in Gamry Echem Analyst. The experimental conditions for zinc electrodeposition are summarized in Table 3.1.

Table 3.1: Experimental conditions of zinc electrodeposition

Test	Constituents	Variable	Concentration (M)	pH	Temperature (^{o}C)	Method
1	Zinc chloride	Control electrolyte	Measured by ICP-OES	Measured by pH meter	25	Chronoamperometry
2	Zinc chloride Potassium chloride	Conductivity salt	Measured by ICP-OES 1.0	Measured by pH meter	25	Chronoamperometry
3	Zinc chloride Boric acid	pH buffer	Measured by ICP-OES 0.5	Measured by pH meter	25	Chronoamperometry
4	Zinc chloride	Temperature	Measured by ICP-OES	Measured by pH meter	45	Chronoamperometry
5	Zinc chloride	pH	Measured by ICP-OES	4.5	25	Chronoamperometry
6	Zinc chloride	Pulsed current	Measured by ICP-OES	Measured by pH meter	25	Repeating chronoamperometry

3.7 Analysis of Zinc Concentration

The concentration of Zn^{2+} ions in each sample was determined using ICP-OES instrument (Optima 7000 DV, Perkin Elmer). First, 1 calibration blank of deionized water and 7 calibration standards of 1, 5, 10, 15, 20, 50, 100 ppm of known Zn^{2+} ions concentrations were prepared to generate the calibration graph. The calibration blank and calibration standards were measured at 5 replicates to obtain the average concentration in each standard.

Then, each sample with unknown concentration of Zn^{2+} ions was measured at three replicates to obtain the average concentration in each sample. A graph of zinc concentration (ppm) versus time (min) was plotted to examine the effects of the six variables on zinc electrodeposition. In addition, zinc recovery was computed by equation (3.4).

$$Zinc\ recovery = \frac{C_2 - C_1}{C_1} \times 100\% \tag{3.4}$$

where

C_1 = Concentration of Zn^{2+} ions in electrolyte solution before electrodeposition, ppm

C_2 = Concentration of Zn^{2+} ions in electrolyte solution after electrodeposition, ppm

3.8 Analysis of Microscopic Structure

The surface microscopic structure of stainless steel electrode after electrodeposition was examined under optical microscope (Olympus BX61) at 1000× magnification. The optical images of stainless steel electrode from different electrolyte conditions were examined to study the changes in microscopic structure after electrodeposition and also to search for zinc deposit.

CHAPTER 4

RESULTS AND DISCUSSION

This chapter discusses the effects of control electrolyte, conductivity salt, pH buffer, electrolyte temperature, electrolyte pH and pulse current on zinc electrodeposition. The discussions are based on the results of ICP-OES, Gamry Echem Analyst and Optical Microscope. The concentration of Zn^{2+} ions in electrolyte solution, the formation of coordination complexes during electrodeposition, the chronoamperometry scan and the microscopic structure of stainless steel electrode after electrodeposition are analyzed accordingly to relate the effects of the six variables on zinc electrodeposition.

4.1 Zinc Adsorption and Desorption

10 % HCl was used as the desorbing agent to desorb Zn^{2+} ions out from activated carbon in a batch desorption for 24 hours. The ICP-OES results showed that less than 10 ppm Zn^{2+} ions were desorbed out even though more than 30 ppm Zn^{2+} ions were adsorbed into activated carbon. The desorption efficiency of HCl was between 20 to 23 %. The concentration of Zn^{2+} ion (ppm) before and after adsorption and desorption is tabulated in Table 4.1.

Table 4.1: Concentration of Zn^{2+} Ion (ppm) before and after Adsorption and Desorption

Sample	Concentration before Adsorption (ppm)	Concentration after Adsorption (ppm)	Concentration in Activated Carbon (ppm)	Concentration after Desorption (ppm)	Desorption Efficiency (%)
1	41.860	8.931	32.929	6.784	20.60
2	49.400	8.158	41.242	9.514	23.07
3	51.550	12.440	39.110	6.498	16.61
4	35.870	5.563	30.307	6.342	20.93

The low desorption efficiency could be attributed to treatment with HCl that increased the surface acidity of activated carbon. This occurred when HCl oxidized the activated carbon surface and dissociated the surface acidic groups. Dissociation of proton (H^+ ion) from the surface functional group resulted in the formation of surface oxygen group ($R\text{-}O^-$) that was negatively charged. This led to stronger electrostatic attraction with the positively charged Zn^{2+} ions. Tseng and Wey (2006) pointed out that HCl treatment could increase deprotonated carboxyl groups on the activated carbon surface and enhance the surface negative charge. In addition, Tan, Ahmad and Hameed (2007) reported an increase in FTIR spectral band of O-H stretching vibrations of carboxylic acid in oil palm shell activated carbon, from 3400 cm^{-1} to 3572 cm^{-1} after treatment with HCl, indicating an increase in surface acidity. HCl enhanced the surface acidity of activated carbon, thereby reducing its desorption efficiency to extract Zn^{2+} ions that were strongly bound to the activated carbon.

4.2 Cyclic Voltammetry

Figure 4.1 shows the cyclic voltammogram of synthetic zinc solution containing 50 ppm zinc and 0.15 M $NaNO_3$. The direction of initial scan was positive at 99.9998 mV/s scan rate. The switching potentials were +1.3 V and –1.3 V. The cycle time was 11:19:50 s.

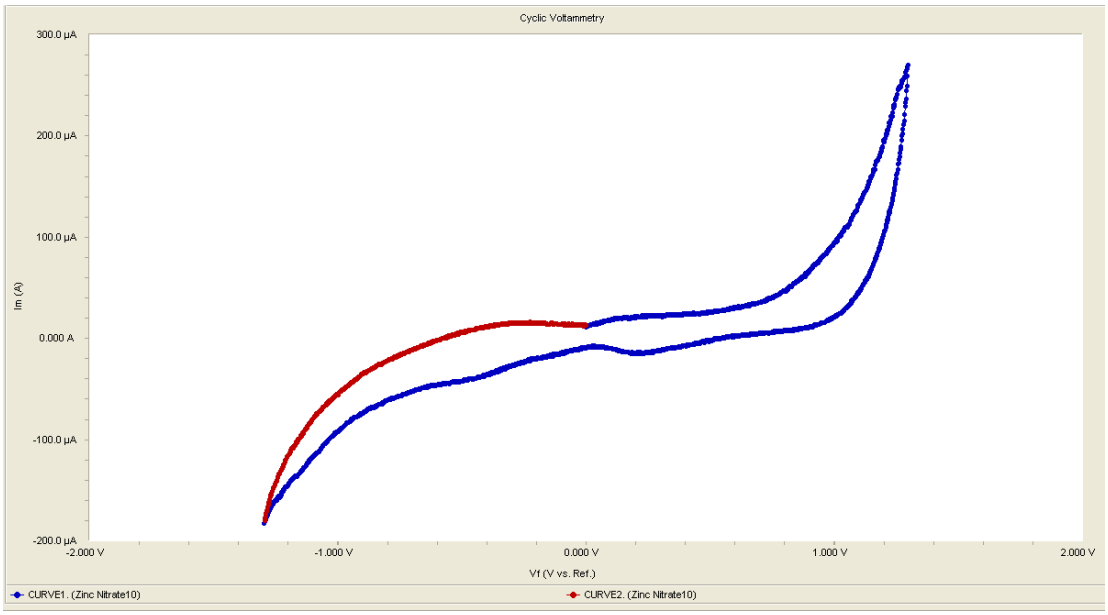

Figure 4.1: Cyclic voltammogram of zinc solution (50 ppm)

First, the potential was reversed scanned in the direction of more positive potentials from 0 V to +1.3 V versus the Ag/AgCl reference electrode. Cathodic current developed between a potential of 0 V to +1.3 V, inferring the reduction of H^+ ions to H_2 gas or Zn^{2+} ions to zinc deposit. Cathodic peak potential E_{pc} at +1.297 V and cathodic peak current i_{pc} at 269.7 µA were observed to be the electrodeposition potential of Zn^{2+} ions.

Then, the potential was forward scanned in the direction of more negative potentials from +1.3 V to –1.3 V versus the Ag/AgCl reference electrode. Anodic current developed between a potential of approximately +0.5 V to –1.3 V, inferring the re-oxidation of zinc deposit to Zn^{2+} ions. Anodic peak potential E_{ac} at –1.295 V and cathodic peak current i_{pc} at –180.0 µA were observed to be the oxidation potential of zinc deposit.

Lastly, the potential was reversed scanned in the direction of more positive potentials from –1.3 V to 0 V versus the Ag/AgCl reference electrode. Cathodic current developed between a potential of approximately –0.6 V to 0 V, inferring the reduction of H^+ ions to H_2 gas or Zn^{2+} ions to zinc deposit.

4.3 Effect of Control Electrolyte

The electrolyte solution consisted of $ZnCl_2$ only without other variables, after Zn^{2+} ions were desorbed from activated carbon by HCl. Figure 4.2 shows a general increase in zinc concentration and decrease in pH over time. Zinc recovery was 0 %.

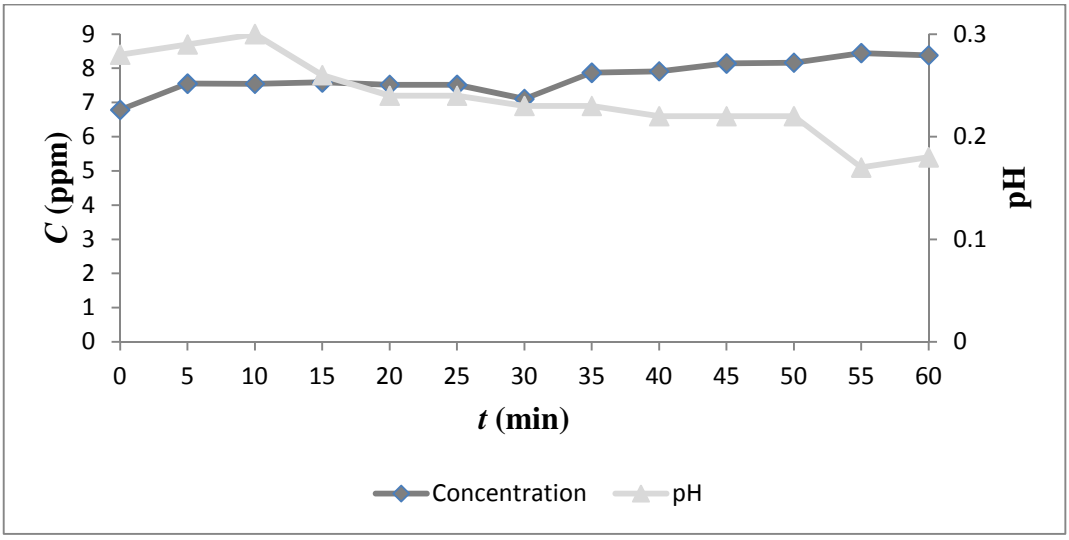

Figure 4.2: Concentration of zinc (ppm) and pH versus time (min)

The results showed that this condition did not favor zinc electrodeposition. Zn^{2+} ions formed a variety of coordination complexes and molecules with Cl^- ions in aqueous solution, which were $Zn(OH)_2$, $Zn(OH)_3^-$, $Zn(OH)_4^{2-}$, Zn_2OH^{3+}, $ZnCl^+$, $ZnCl_2$, $(ZnCl_3)^-$, $(ZnCl_4)^{2-}$ and $ZnOH^{+,}$ as modeled by Visual MINTEQ (KTH). Dissociation of coordination complexes was required to release metallic cations for discharge (Gabe, 1978). The results suggested that Zn^{2+} ions were bound in stable coordination complexes and molecules which inhibited electrodeposition.

The increase in zinc concentration could be due to the oxidation of OH^- and Cl^- ions to O_2 and Cl_2 gas at the counter electrode. Zn^{2+} ions became concentrated as OH^- and Cl^- ions were removed from the electrolyte solution. In addition, removal of OH^- ions also caused the decrease in electrolyte pH with time. Therefore, another deduction could be made based on this relation. Zincate complexes had to dissociate to release free Zn^{2+} and OH^- ions to balance the removal of OH^- ions at the counter electrode, and hence the electrolyte pH increased in the first 10 minutes. However,

zinc electrodeposition did not occur, suggesting that free Zn^{2+} ions that were released by dissociation of zincate complexes had higher tendency to form zinc chloride complexes with Cl^- ions than being reduced at the working electrode. The decrease in electrolyte pH after 10 minutes inferred that zincate complexes were present in smaller amount as these complexes were fully dissociated and hence no free OH^- ions to increase the electrolyte pH after 10 minutes. Therefore, the dominant complex species in this electrolyte system were zinc chloride coordination complexes which were present in larger amount.

Figure 4.3 shows the chronoamperometry scan of control electrolyte. The potential (blue curve) rose but remained at negative value. The potential did not reach the electrodeposition potential of zinc at +1.297 V, confirming no reduction of Zn^{2+} ions to zinc deposit. Redistribution of the electrode potential was caused by the presence of coordination complexes that altered the reduction behavior of Zn^{2+} ions (Xu et al., 2015). In contrast, the current (green curve) remained constant at positive value.

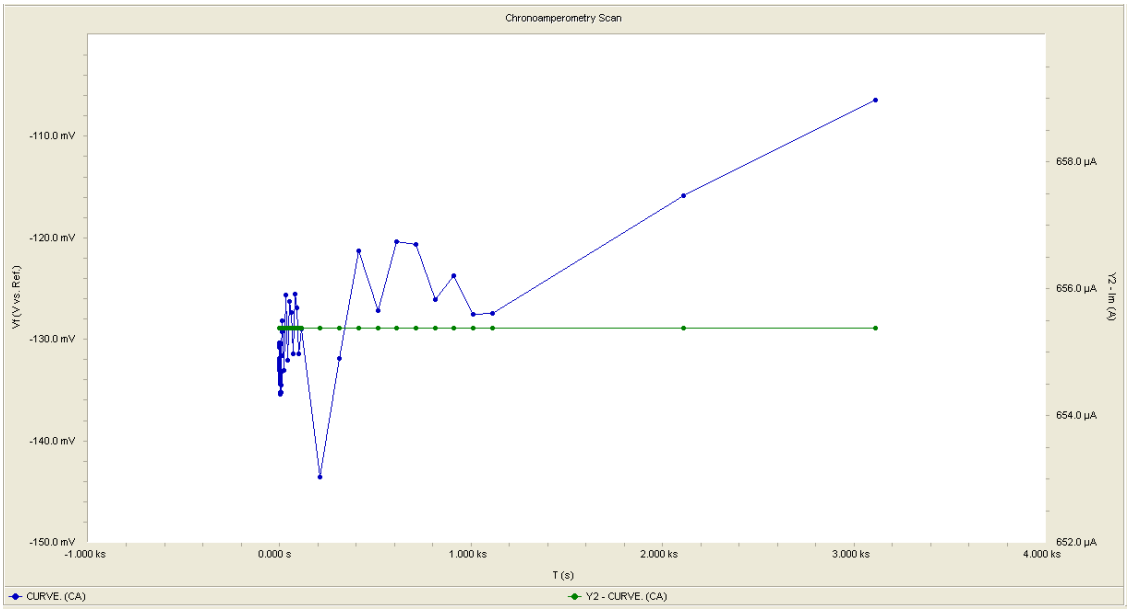

Figure 4.3: Chronoamperometry scan of control electrolyte

Although positive potential (+1.297 V) was applied, the chronoamperometry scan in Figure 4.3 shows that the potential versus Ag/AgCl reference electrode was

negative. Abbott et al. (2011) stated that metallic ions in ionic liquid produced anionic species. The concentration of metallic ions at the electrode surface decreased at more negative applied potential, due to the formation of cationic layer that inhibited the diffusion of anionic metallic species to the electrode surface. Hence, it could be deduced that cationic layer was formed at the stainless steel electrode surface that hindered the diffusion of anionic zinc complexes to the electrode surface. As a result, these complexes could not be dissociated by electrolysis to release free Zn^{2+} ions for electrodeposition.

Figure 4.4 illustrates the optical image of stainless steel electrode before chronoamperometry. Intergranular corrosion could be observed along the grain boundaries. This occurred when chromium and carbon diffused to the grain boundaries and formed chromium carbide $Cr_{23}C_6$ precipitates, leaving a chromium depleted zone next to the grain boundary that was susceptible to corrosion (Callister and Rethwisch, 2011). Figure 4.4 was used as the standard to compare with the optical images of stainless steel electrode after subjected to chronoamperometry at different electrolyte conditions.

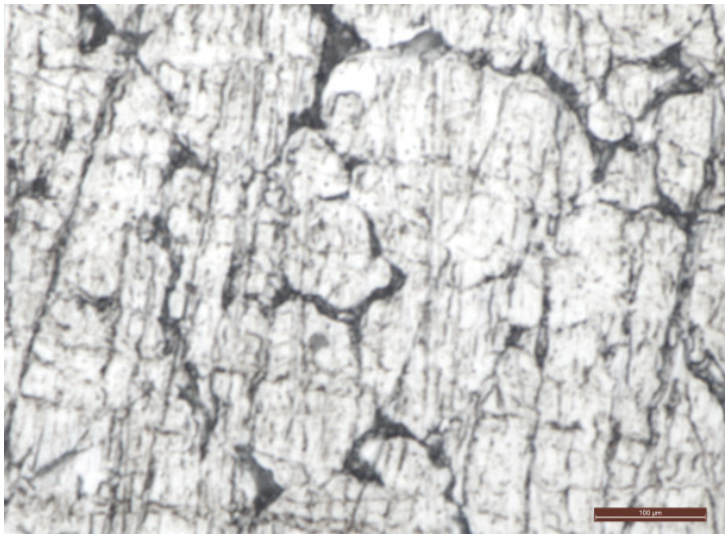

Figure 4.4: Optical image of stainless steel electrode at 1000 × magnification

Figure 4.5 illustrates the optical image of stainless steel electrode of control electrolyte. The microscopic structure consisted of coarse grains with uneven size because stainless steel electrode was corroded by the acidic electrolyte solution. The

colour of electrolyte solution was observed to change from colourless to green, which could be related to the corrosion of stainless steel electrode. Chromium in stainless steel electrode dissolved into the electrolyte solution as chromium ions Cr^{3+}, possibly forming chromium(III) chloride $CrCl_3(H_2O)_x$ or hydrated chromium ions $[Cr(H_2O)_6]^{3+}$ which caused the electrolyte solution to turn green. Therefore, the negative potential in chronoamperometry scan could be due to the oxidation of chromium to Cr^{3+} ion at the working electrode.

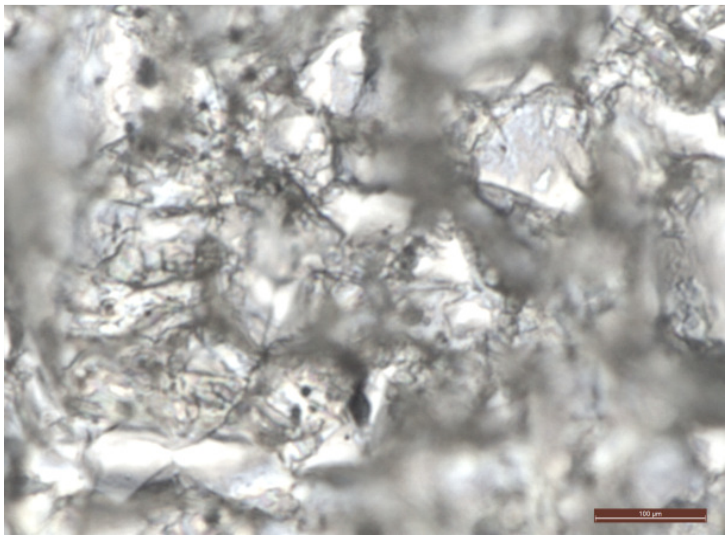

Figure 4.5: Optical image of stainless steel electrode at 1000 × magnification

4.4 Effect of Potassium Chloride

The electrolyte solution consisted of $ZnCl_2$ and 1.0 M KCl. Figure 4.6 shows a general decrease in zinc concentration and electrolyte pH. Zinc concentration started to drop after 20 minutes. Zinc recovery was 62.19 %, where its concentration reduced from 9.514 to 3.597 ppm.

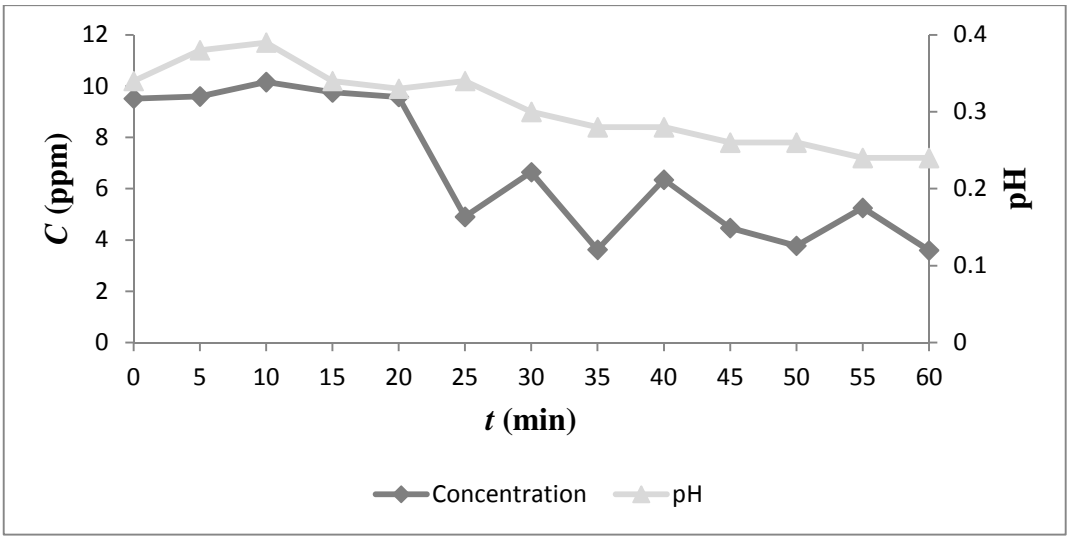

Figure 4.6: Concentration of zinc (ppm) and pH versus time (min) for electrolyte containing $ZnCl_2$ and 1.0 M KCl

The results showed that this condition favored zinc electrodeposition. KCl acted as conductivity salt by dissociating into K^+ and Cl^- ions, thereby increasing the electrical conductivity of electrolyte solution. Reduction and oxidation could occur more readily at the electrodes in the presence of large quantities of easily dissociated ions which accelerated electron transfer. Therefore, reduction of Zn^{2+} ions to zinc deposit occurred more readily. The stability of Zn^{2+} ions bound to the coordination complexes and molecules was overcome by the effects of KCl on the electrolyte system. In addition, KCl acted as weak ligands of Zn^{2+} ions by forming the high coordination complex $K_4(ZnCl_6)$ (Yu et al., 2013). These weak ligands could be easily dissociated from the coordination complex to release free Zn^{2+} for electrodeposition.

Besides, KCl acted as an inert supporting electrolyte that minimized the migration of ions under the influence of electric field between the working and counter electrode (Skoog et al., 2004). Migration caused attraction of anions to the positive counter electrode and cations to the negative working electrode. This charge movement constituted a current to complete the electrical circuit. The resulting effect was passivation of the negative working electrode with cationic layer, which was in agreement with the theory proposed by Abott et al. (2011) as mentioned in section 4.3. As a result, anionic metallic species could not diffuse and discharge at the

electrode surface. In the presence of KCl, K^+ and Cl^- ions carried the charges to sustain the current flow instead of ion migration. Hence, the passivation of electrode surface with cationic layer was reduced and anionic zinc complexes could diffuse more readily to the electrode surface for discharge.

However, the electrolyte pH was higher than control electrolyte because potassium, as an alkali metal, increased the electrolyte pH. Removal of OH^- ions as O_2 gas caused the decrease in electrolyte pH with time.

Figure 4.7 shows the chronoamperometry scan for $ZnCl_2$ in 1.0 M KCl. The potential (blue curve) rose but remained at negative potential. Although the potential did not reach +1.297 V, zinc electrodeposition was facilitated by the conductivity salt. In addition, Figure 4.7 shows different trend compared to Figure 4.3 (control), suggesting that KCl had significant effect on the electrolyte resistance. The current (green curve) remained constant at positive value.

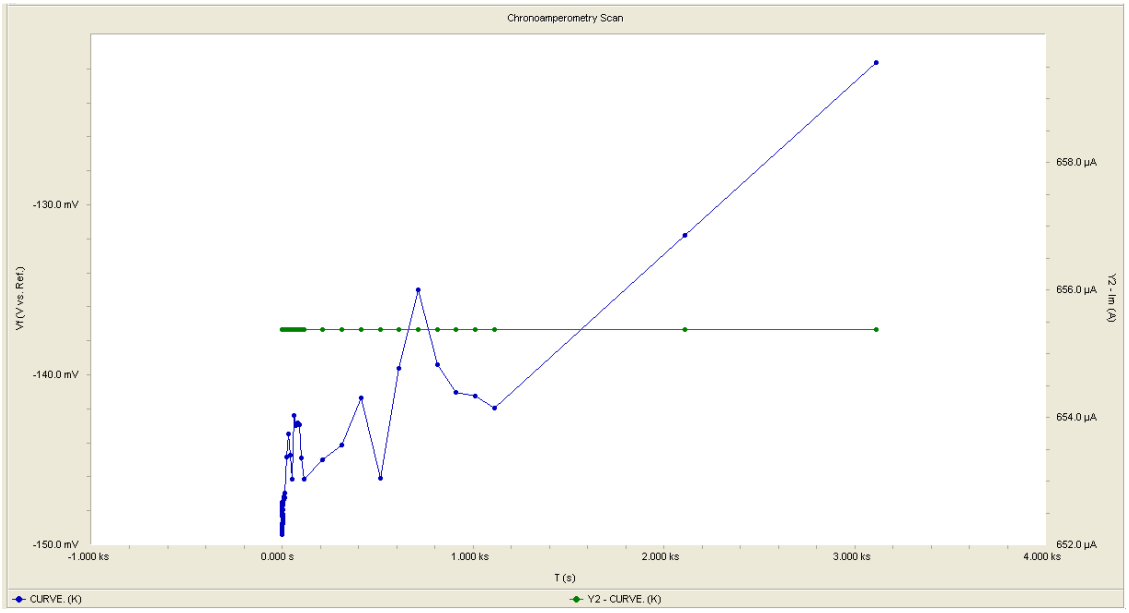

Figure 4.7: Chronoamperometry scan for $ZnCl_2$ in 1.0 M KCl

Figure 4.8 illustrates the optical images of stainless steel electrode of electrolyte containing $ZnCl_2$ and 1.0 M KCl. The microscopic structure also consisted of coarse grains with uneven size due to corrosion of stain steel electrode.

Besides, the colour of electrolyte solution changed from colourless to green as explained in section 4.3. Although Figure 4.6 showed that zinc electrodeposition occurred, zinc deposit was not visible under the resolution of optical microscope since only 5.917 ppm zinc was recovered according to ICP-OES measurement.

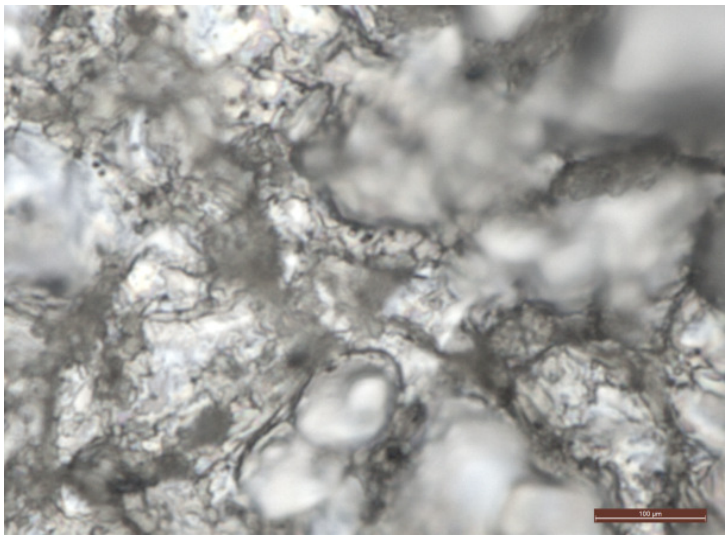

Figure 4.8: Optical image of stainless steel electrode at 1000 × magnification of electrolyte containing $ZnCl_2$ and 1.0 M KCl

4.5 Effect of Boric Acid

The electrolyte solution consisted of $ZnCl_2$ and 0.5 M boric acid. Figure 4.9 shows a random variation in zinc concentration and decrease in electrolyte pH with time. The initial zinc concentration was lower than the final zinc concentration. Zinc recovery was 0 %.

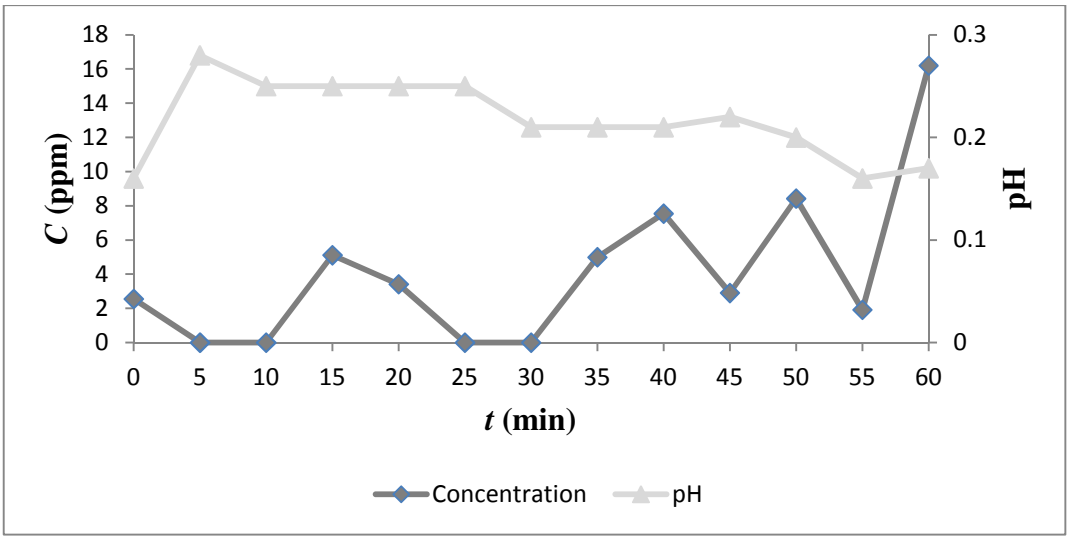

Figure 4.9: Concentration of zinc (ppm) and pH versus time (min) for electrolyte containing $ZnCl_2$ and 0.5 M boric acid

The results showed that this condition did not favor zinc electrodeposition. Zn^{2+} ions formed different coordination complex and molecule in the presence of boric acid, which were $Zn(H_2BO_3)_2$ and $ZnH_2BO_3^+$. These complex ions and molecules could have introduced spectral interferences during ICP-OES measurement of zinc concentration. Spectral interferences were caused by excitation of multi elements in highly complex samples that produced rich spectra (Meyers, 2000). Zn^{2+} ions were bound in stable coordination complexes which inhibited electrodeposition. These coordination complex and molecule could have dissociated by electrolysis into simpler ions, hence less spectral interferences in samples collected after 30 minutes and ICP-OES detected higher zinc concentration. However, the coordination complexes were stable enough to inhibit zinc electrodeposition.

Boric acid acted as pH buffer to maintain the electrolyte pH. This was observed between 10^{th} to 25^{th} minutes in which the electrolyte pH was maintained at 0.25, and between 30^{th} to 40^{th} minute in which the electrolyte pH was maintained at 0.21. In general, removal of OH^- ions as O_2 gas caused the decrease in electrolyte pH with time. This could be related to the increase in zinc concentration. When the electrolyte pH decreased, more H^+ ions were present and the equilibrium in equation (2.5) shifted to the right where $(BO_3)^{3-}$ ions were converted to H_3BO_3 molecules. Fewer $(BO_3)^{3-}$ ions formed coordination complexes and molecules with Zn^{2+} ions,

hence less spectral interferences in samples collected after 30 minutes and ICP-OES measurement detected higher zinc concentration.

Figure 4.10 shows the chronoamperometry scan for $ZnCl_2$ in 0.5 M boric acid. There was drastic difference compared to Figure 4.3 (control electrolyte) and Figure 4.9 (potassium chloride). The potential (blue curve) dropped between 0 to 300th s (5th minutes), probably due to dissociation of $Zn(H_2BO_3)_2$ and $ZnH_2BO_3^+$ complexes. The potential did not attain +1.297 V, confirming no reduction of Zn^{2+} ions to zinc deposit. The negative potential could be explained by oxidation of chromium in stainless steel to Cr^{3+} ions, which caused the electrolyte solution to turn green. The current (green curve) remained constant at positive value.

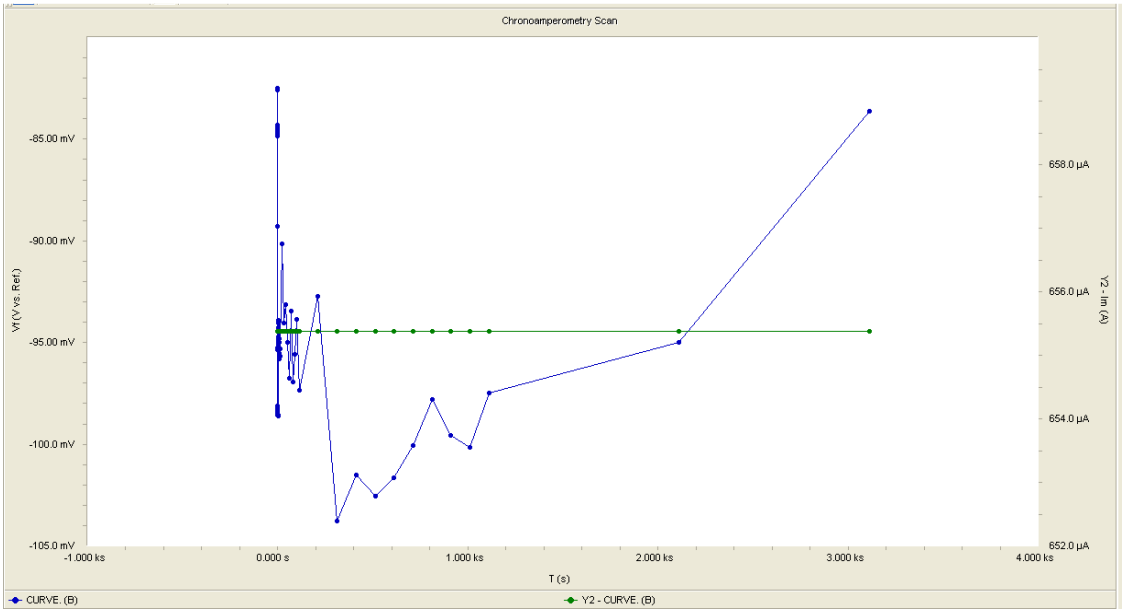

Figure 4.10: Chronoamperometry scan for $ZnCl_2$ in 0.5 M boric acid

Figure 4.11 illustrates the optical image of stainless steel electrode of electrolyte containing $ZnCl_2$ and 0.5 M boric acid. The microscopic structure also consisted of coarse grains with uneven size due to corrosion of stain steel electrode. Besides, the colour of electrolyte solution changed from colourless to green as explained in section 4.3.

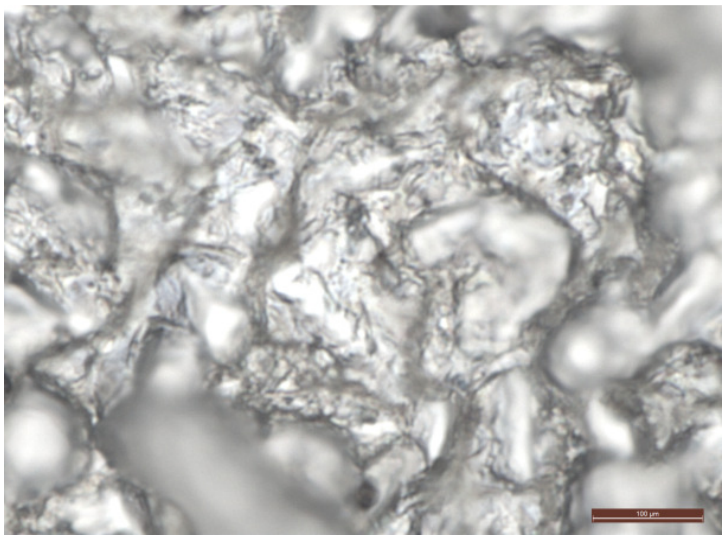

Figure 4.11: Optical image of stainless steel electrode at 1000 × magnification of electrolyte containing $ZnCl_2$ and 0.5 M boric acid

4.6 Effect of pH

The electrolyte solution consisted of $ZnCl_2$ and sodium hydroxide NaOH at pH 4.5. Figure 4.12 shows a decrease in zinc concentration and increase in electrolyte pH with time. Zinc concentration started to drop sharply after 5 minutes. Zinc recovery was 100 %, where its concentration reduced from 6.498 to 0 ppm in 15 minutes.

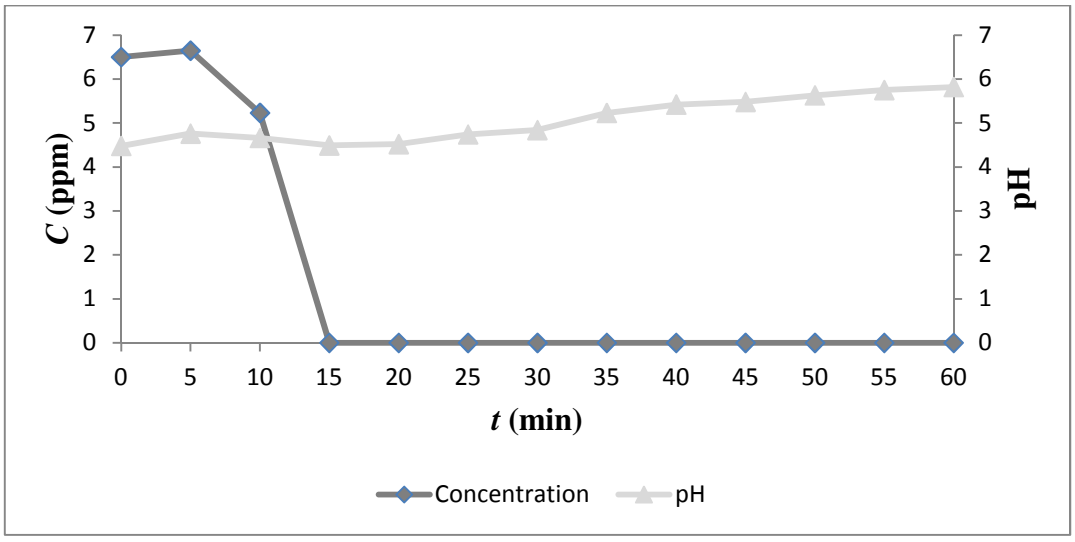

Figure 4.12: Concentration of zinc (ppm) and pH versus time (min) for electrolyte at pH 4.5

The results showed that this condition favored zinc electrodeposition. The increase in electrolyte pH indicated the presence of more free OH^- ions in the electrolyte solution. This suggested that zinc electrodeposition occurred mainly through dissociation of zincate complexes instead of zinc chloride complexes, which released free Zn^{2+} ions for electrodeposition and free OH^- ions that increased the electrolyte pH. In addition, it could be deduced that pH between 4.5 and 6 favored the formation of zincate complexes which provided free Zn^{2+} ions for electrodeposition.

Figure 4.13 shows the chronoamperometry scan of electrolyte at pH 4.5. The potential (blue curve) remained at +1.297 V, confirming reduction of Zn^{2+} ions to zinc deposit. The current (green curve) remained constant at positive value. It could be deduced that the positive applied potential (+1.297 V) at working electrode promoted the formation of anionic layer that consisted of anionic zinc complexes. This inferred that free Zn^{2+} ions were easily dissociated from anionic complexes compared to cationic complexes. This inference could also be related to the results in section 4.3. The control electrolyte system was dominated by cationic layer at the electrode surface, suggesting that free Zn^{2+} ions were not easily dissociated from the stable cationic complexes.

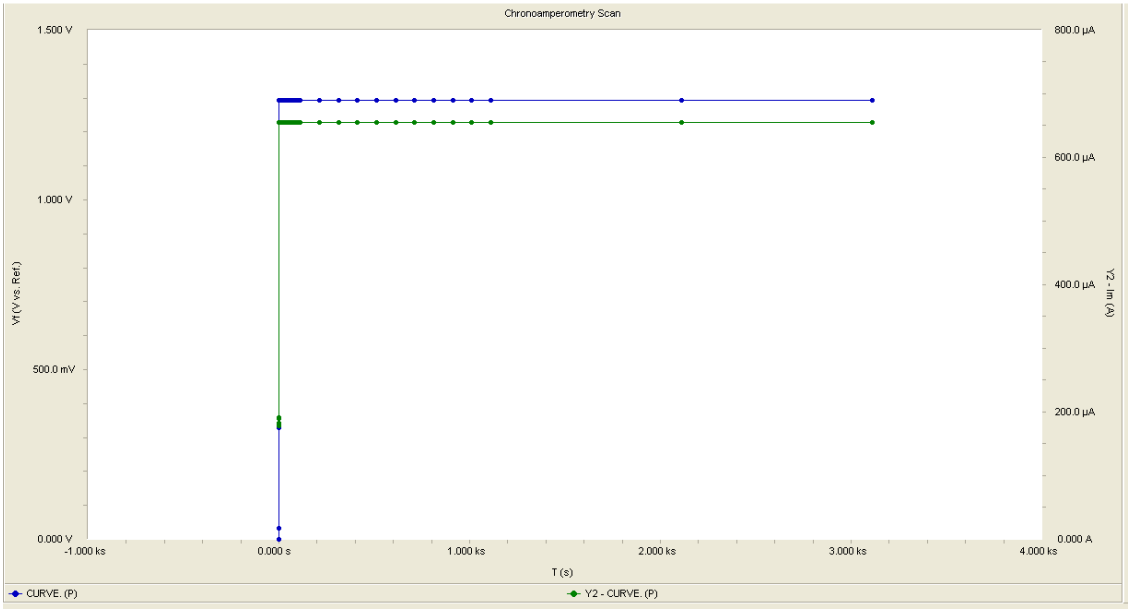

Figure 4.13: Chronoamperometry scan of electrolyte at pH 4.5

Figure 4.14 illustrates the optical image of stainless steel electrode of electrolyte at pH 4.5. The microscopic structure consisted of numerous grain boundaries with intergranular corrosion. The black hole was pitting corrosion on the electrode surface. Zinc deposit was not visible under the resolution of optical microscope since only 6.498 ppm zinc was recovered according to ICP-OES measurement.

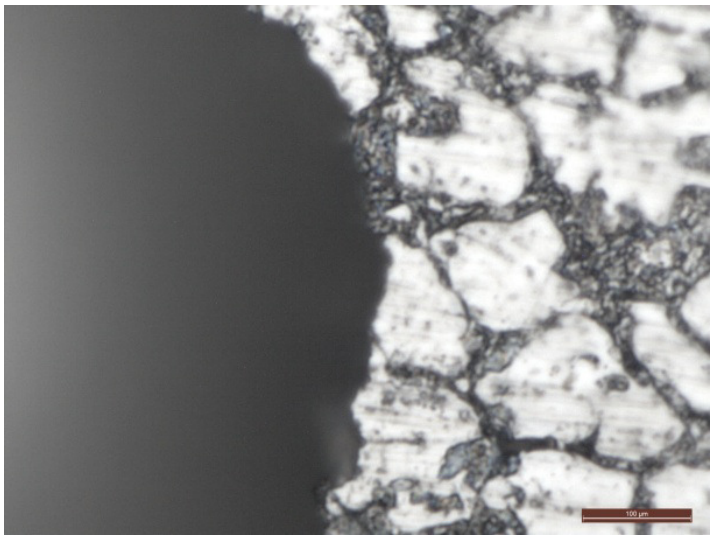

Figure 4.14: Optical image of stainless steel electrode at 1000 × magnification of electrolyte at pH 4.5

4.7 Effect of Temperature

The electrolyte solution consisted of $ZnCl_2$ only at 45^{o}C. Figure 4.15 shows that zinc concentration increased between 0 to 15th minutes, decreased between 15th to 25th minutes and maintained between 25th to 60th minutes. In general, the electrolyte pH decreased with time. Zinc recovery was 0 %.

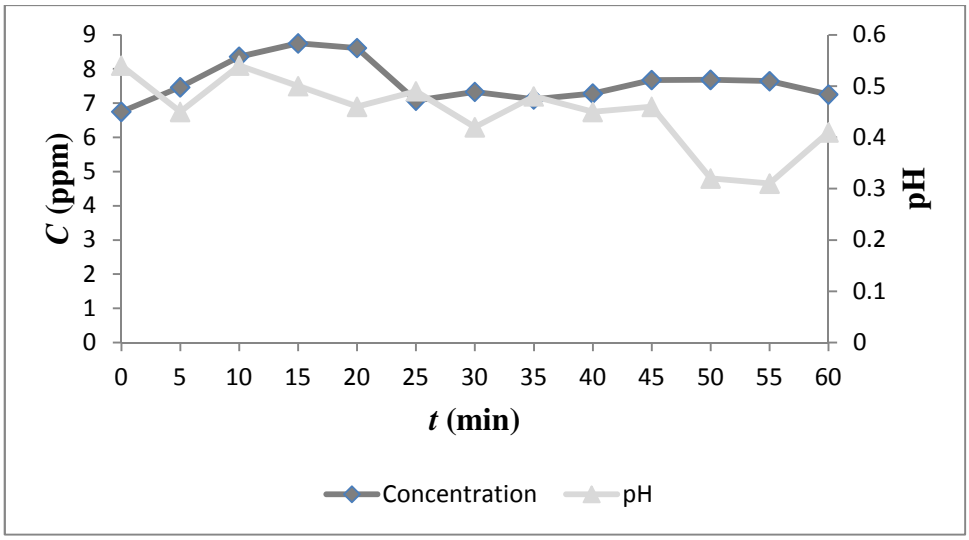

Figure 4.15: Concentration of zinc (ppm) and pH versus time (min) for electrolyte at 45°C

The results showed that this condition did not favor zinc electrodeposition. This suggested that electrolyte temperature of 45°C did not influence dissociation of Zn^{2+} ions bound in stable coordination complexes and molecules which in turn inhibited Zn electrodeposition. However, the electrolyte pH was higher compared to the results shown in Figure 4.2 (control electrolyte), Figure 4.6 (potassium chloride) and Figure 4.9 (boric acid), inferring that temperature increased free OH^- ions in this electrolyte system. Removal of OH^- ions as O_2 gas caused the decrease in electrolyte pH over time.

Figure 4.16 shows the chronoamperometry scan of electrolyte at 45°C. The potential (blue curve) varied randomly. This indicates that higher temperature could affect mass transfer rate of ions and electrolyte conductivity. The potential reached +1.297 V but did not maintain at that value because high temperature had significant effect on the electrolyte conductivity; hence Zn^{2+} ions were unable to reduce to zinc deposit. The current (green curve) remained constant at positive value.

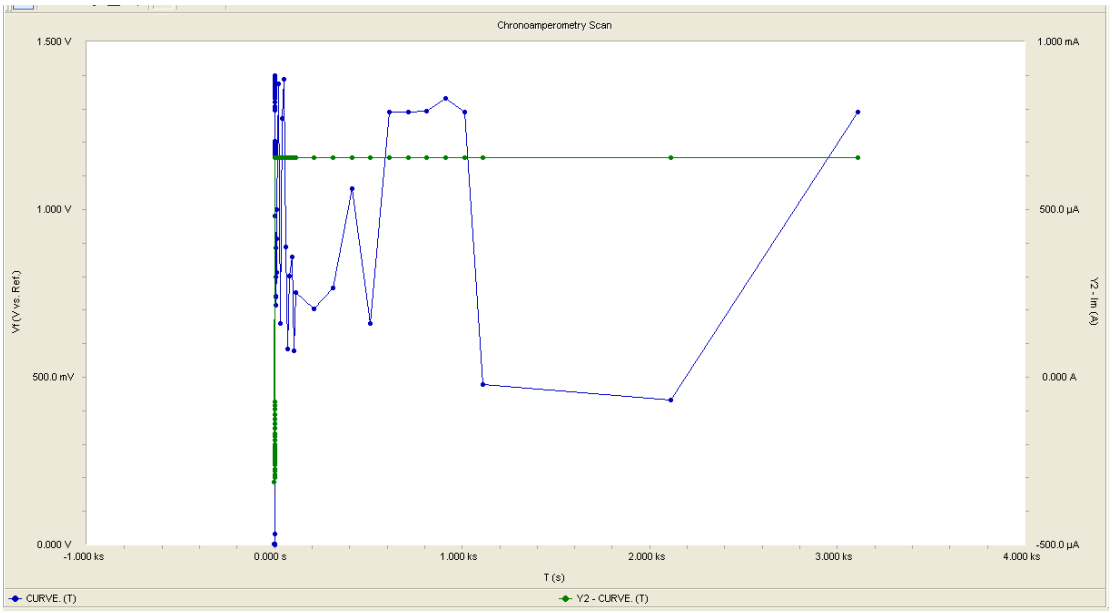

Figure 4.16: Chronoamperometry scan of electrolyte at 45^{o}C

Figure 4.17 illustrates the optical image of stainless steel electrode of electrolyte at 45^{o}C. The microscopic structure consisted of coarse grains with uneven size due to corrosion of stain steel electrode. Corrosion of electrode could be enhanced at higher temperature (Gamburg and Zangari, 2011). Besides, the colour of electrolyte solution changed from colourless to green as explained in section 4.3.

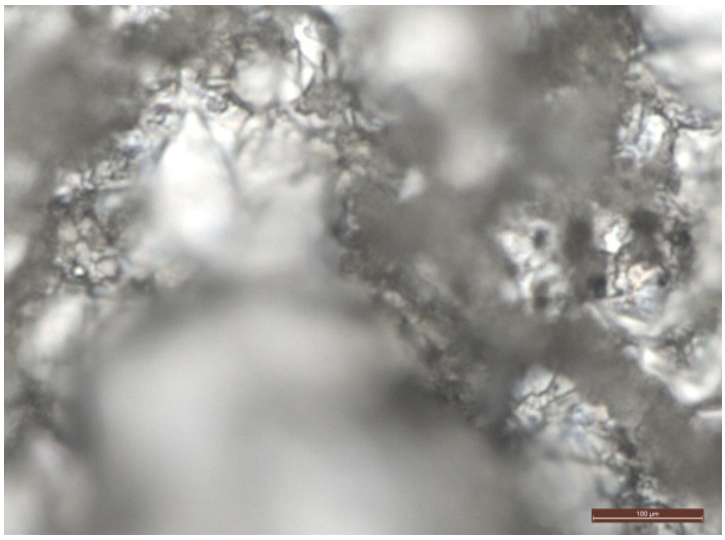

Figure 4.17: Optical image of stainless steel electrode at 1000 × magnification of electrolyte at 45 ^{o}C

4.8 Effect of Pulse Current

The electrolyte solution consisted of $ZnCl_2$ only subjected to repeating chronoamperometry. Figure 4.18 shows a general increase in zinc concentration and decrease in pH over time. Zinc recovery was 0 %.

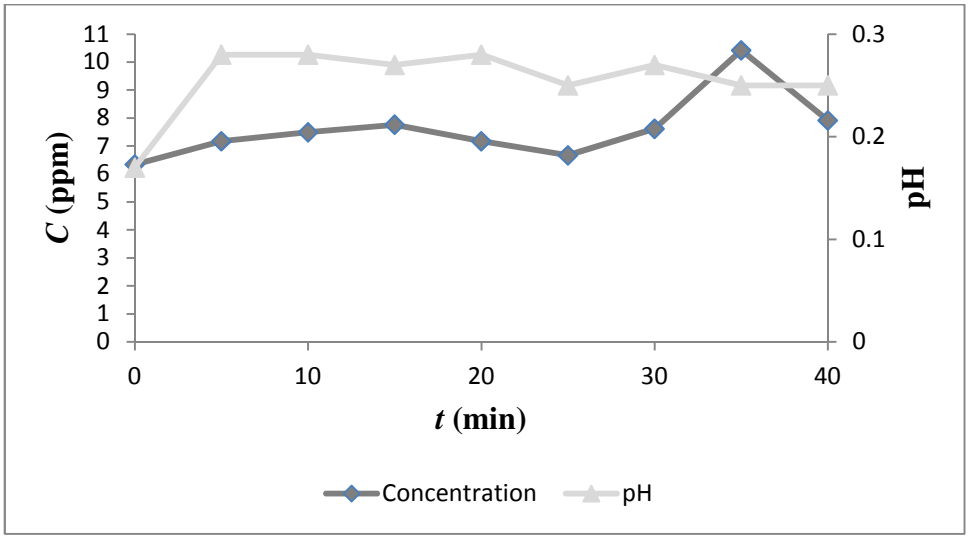

Figure 4.18: Concentration of zinc (ppm) and pH versus time (min) for electrolyte subject to pulsed current

The results showed that this condition did not favor zinc electrodeposition. The situation was rather similar to the control electrolyte. Zn^{2+} ions were bound in stable coordination complexes and molecules which inhibited electrodeposition. Pulse current could not dissociate the stable zincate complexes to release free Zn^{2+} ions for electrodeposition. Removal of OH^- ions as O_2 gas caused the decrease in electrolyte pH with time.

Figure 4.19 shows the chronoamperometry scan of electrolyte subjected to pulse current. The potential (blue curve) stepped up to +1.297 V for 5 s and step down to 0 V for 5 s repeatedly. Although the potential attained at +1.297 V, zinc electrodeposition did not occurr, inferring that the conditions of electrolyte solution (constituents and pH) had stronger effect on zinc electrodeposition. The current (green curve) remained constant at positive value.

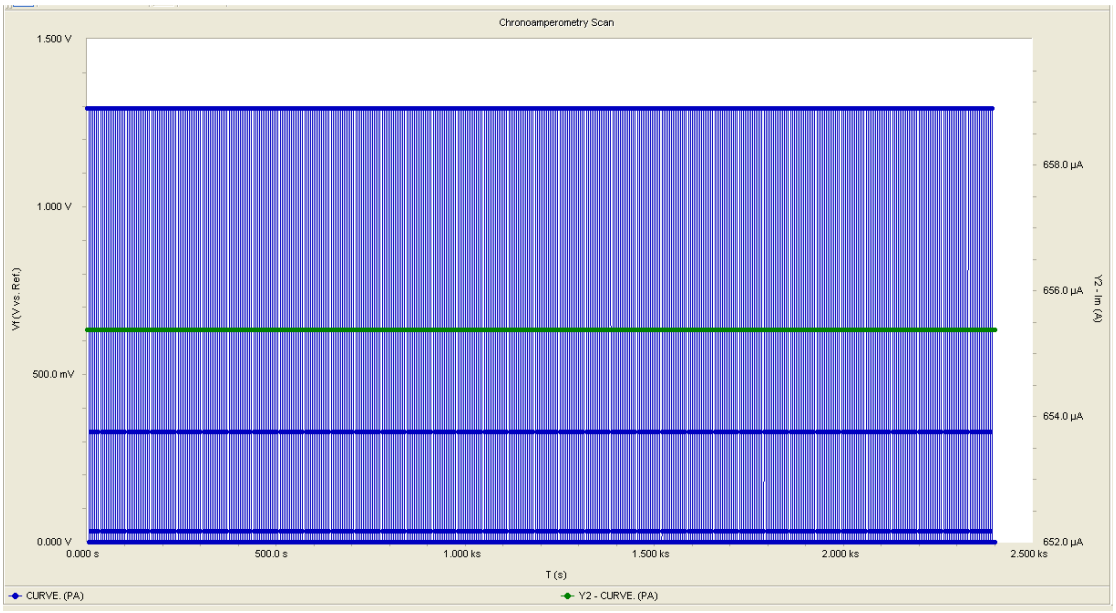

Figure 4.19: Chronoamperometry scan of electrolyte subjected to pulse current

Figure 4.20 illustrates the optical image of stainless steel electrode of electrolyte at 45^{o}C. The microscopic structure consisted of coarse grains with uneven size due to corrosion of stain steel electrode. Besides, the colour of electrolyte solution changed from colourless to green as explained in section 4.3.

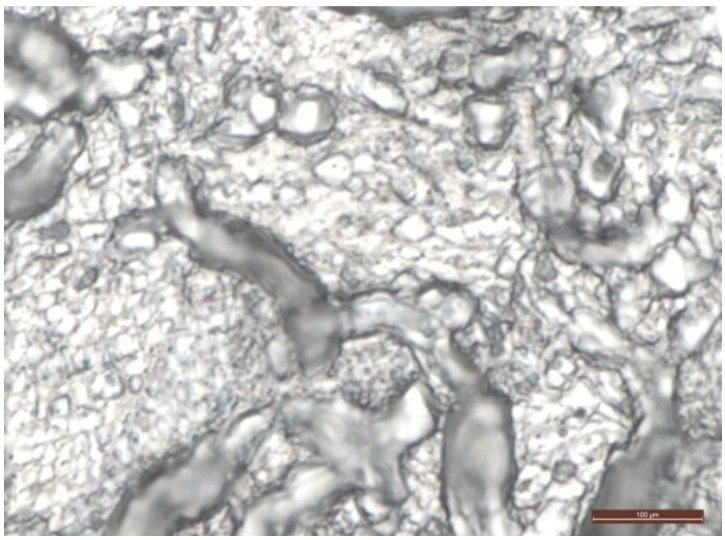

Figure 4.20: Optical image of stainless steel electrode at 1000 × magnification of electrolyte subject to pulse current

CHAPTER 5

CONCLUSION AND RECOMMENDATIONS

5.1 Conclusion

This research project studied the application of electrochemical methods in wastewater treatment. Zn^{2+} ions in synthetic solution were removed by adsorption onto palm shell activated carbon and then desorbed by HCl acid. The HCl solution containing desorbed Zn^{2+} ions was used for cyclic voltammetry and chronoamperometry experiments.

The desorption efficiency of 10 % HCl was between 20 to 23 %. The low desorption efficiency was due to HCl treatment on palm shell activated carbon, which increased its surface acidity by dissociation of proton from the surface functional group. This led to the formation of negatively-charged surface oxygen group that formed stronger electrostatic attraction with Zn^{2+} ions, thus reducing their desorption.

Zinc electrodeposition was studied using cyclic voltammetry experiment. Cyclic voltammetry determined that the electrodeposition potential of zinc was +1.297 V. In chronoamperometry experiments, the effects of control electrolyte, conductivity salt, pH buffer, electrolyte pH, electrolyte temperature and pulse current on zinc electrodeposition were studied to determine the optimum parameters for electrochemical zinc recovery.

Among the six parameters, electrolyte at pH 4.5 showed 100 % zinc recovery after 15 minutes. The result suggested that zinc electrodeposition occurred through dissociation of zincate complexes, which released free Zn^{2+} ions for electrodeposition and free OH^- ions that increased the electrolyte pH. Besides, the result proposed that free Zn^{2+} ions were easily dissociated from anionic zincate complexes compared to cationic complexes, in which the electrode surface was dominated by anionic layer at positive applied potential (+1.297 V)

On the other hand, electrolyte solution containing KCl conductivity salt showed 62.19 % zinc recovery in 60 minutes. KCl enhanced the electrical conductivity of electrolyte solution, thereby accelerating reduction and oxidation at the electrodes. KCl also formed $K_4(ZnCl_6)$ complexes that easily released free Zn^{2+} ions for electrodeposition because KCl was a weak ligands to Zn^{2+} ions. In addition, KCl reduced ion migration and subsequently passivation of the electrode surface with cationic layer to promote diffusion of anionic zinc complexes to the electrode surface for discharge.

Control electrolyte, boric acid, electrolyte temperature at 45^oC and pulse current exhibited 0 % zinc recovery. These conditions did not favor zinc electrodeposition due to the presence of stable coordination complexes and molecules that strongly bound free Zn^{2+} ions and inhibited electrodeposition.

5.2 Recommendations

Zinc desorption from palm shell activated carbon can be studied using different acids with different concentrations, such as nitric acid or sulphuric acid. This research project showed that electrolyte pH at 4.5 was the optimum condition for 100 % zinc recovery. Therefore, acid with the highest desorption efficiency at the lowest concentration is desirable to reduce the amount of alkali used for adjusting the electrolyte pH.

REFERENCES

Agency for Toxic Substances and Disease Registry, 2005. *Public health statement for zinc*. [online] Available at: <http://www.atsdr.cdc.gov/PHS/PHS.asp?id=300&tid=54> [Accessed 20 June, 2014].

Bansal, R.C. and Goyal, M., 2005. *Activated carbon adsorption*. [e-book] USA: CRC Press. Available at: Google Books <books.google.com> [Accessed 20 June, 2014].

Barakat, M.A., 2011. New trends in removing heavy metals from industrial wastewater. *Arabian Journal of Chemistry*, 4(4), pp. 361-377.

Brankovic, S. and Rajeshwar, K. eds., 2008. *Electrodeposition for energy applications*. [e-book] New Jersey: The Electrochemical Society. Available at: Google Books <books.google.com> [Accessed 27 June, 2014].

Callister Jr., W.D. and Rethwisch, D.G., 2011. *Materials science and engineering*. 8th ed. Asia: John Wiley & Sons Pte ltd.

Campbell, F.C. ed., 2008. *Elements of Metallurgy and Engineering Alloys*. [e-book] USA: ASM International. Available at: Google Books <books.google.com> [Accessed 28 July, 2014].

Chen, G., 2004. Electrochemical technologies in wastewater treatment. *Separation and Purification Technonlogy*, 38(1), pp. 11-41.

Fu, F. and Wang, Q., 2010. Removal of heavy metal ions from wastewaters: A review. *Journal of environmental management*, 92(2011), pp. 407-418.

Gabe, D.R., 1978. *Principles of metal surface treatment and protection*. 2nd ed. [e-book] London: Cox & Wyman Ltd. Available at: Google Books <books.google.com> [Accessed 19 March, 2014].

Gamburg, Y.D. and Zangari, G. eds., 2011. *Theory and practice of metal electrodeposition*. [e-book] New York: Springer. Available at: Google Books <books.google.com> [Accessed 29 June, 2014].

Ghanbari, F. and Moradi, M., 2015. A comparative study of electrocoagulation, electrochemical Fenton, electro-Fenton and peroxi-coagulation for decolorization of real textile wastewater: Electrical energy consumption and biodegradability improvement. *Journal of Environmental Chemical Engineering*, 3(1), pp. 499-506.

Gonzalez, P.G. and Pliego-Cuervo, Y.B., 2014. Adsorption of Cd(II), Hg(II) and Zn(II) from aqueous solution using mesoporous activated carbon produced from *Bambusa vulgaris striata*. *Chemical Engineering Research and Design*, 92(2014), pp. 2715-2724.

Jensen, O.M. ed., 2009. *The science of construction materials*. [e-book] New York: Springer. Available at: Google Books <books.google.com> [Accessed 20 July, 2014].

Lewinsky, A.A. ed., 2007. *Materials and wastewater: Treatment, removal and analysis*. [e-book] New York: Nova Science Publishers, Inc. Available at: Google Books <books.google.com> [Accessed 30 July, 2014].

Liu, C.X., Hu, Z.Q., Zuo, J.L., Hu, M. and Xiao, B., 2014. Removal of Zn(II) from Simulated Wastewater Using an Algal Biofilm. *Water Science and Technology*, 70(8), pp. 1383-1390.

Loto, C.A. and Loto, R.T., 2013. Effect of dextrin and thiourea additives on the zinc electroplated mild steel in acid chloride solution. *Int. J. Electrochem. Sci.*, 8(2013), pp. 12434-12450.

Mansoorian, H.J., Mahvi, A.H. and Jafari, A.J., 2014. Removal of lead and zinc from battery industry wastewater using electrocoagulation process: Influence of direct and alternating current by using iron and stainless steel rod electrodes. *Separation and Purification Technology*, 135(2014), pp. 165-175.

Masters, G.M. and Ela, W.P., 2008. *Introduction to environmental engineering and science*. 3rd ed. Upper Saddle River: Pearson Prentice Hall.

Meyers., R.A. ed., 2000. *Encyclopedia of analytical chemistry*. Asia: John Wiley & Sons Pte ltd.

Mook, W.T., Aroua, M.K. and Issabayeva, G., 2014. Prospective applications of renewable energy based electrochemical systems in wastewater treatment: A review. *Renewable and Sustainable Energy Reviews*, 38(2014), pp. 36-46.

Naik, Y.A., Venkatesha, T.V. and Nayak, P.V., 2001. Electrodeposition of zinc from chloride solution. *Turk J Chem*, 26(2002), pp. 725-733.

Paduraru, C., Tofan, L., Teodosiu, C., Bunia, I., Tudorachi, N. and Toma, O., 2014. Biosorption of zinc(II) on rapeseed waste: Equilibrium studies and thermogravimetric investigations. *Process Safety and Environmental Protection*, 94(2015), pp. 18-28.

Porter, F.C. ed., 1991. *Zinc handbook: properties, processing and use in design*. [e-book] New York: Marcel Dekker, Inc. Available at: Google Books <books.google.com> [Accessed 18 June, 2014].

Rahmanian, B., Pakizeh, M. and Maskooki, A., 2010. Micellar-enhanced ultrafiltration of zinc in synthetic wastewater using spiral-wound membrane. *Journal of Hazardous Materials*, 184(2010), pp. 261-267.

Rao, M.M., Rao, G.P.C., Seshaiah, K., Choudary, N.V. and Wang, M.C., 2007. Activated carbon from Ceiba pentandra hulls, an agricultural waste, as an adsorbent in the removal of lead and zinc from aqueous solutions. *Waste Management*, 28(2008), pp. 849-858.

Saber, K., Koch, C.C. and Fedkiw, P.S., 2001. Pulse current electrodeposition of nanocrystalline zinc. *Material Science and Engineering*. A341(2003), pp. 174-181.

Skoog, D.A., West, D.M., Holler, F.J. and Crouch, S.R., 2004. *Fundamentals of analytical chemistry*. 8th ed. Belmont: Thomson Brooks/Cole.

Sullivan, J.B.Jr. and Krieger, G.R. eds., 2001. *Clinical Environmental Health and Toxic Exposures*. 2nd ed. [e-book] USA: LIPPINCOTT WILLIAMS $ WILKINS. Available at: Google Books <books.google.com> [Accessed 30 August, 2014].

Xu, M., Ivey, D.G., Qu, W. and Xie, Z., 2015. Study of the mechanism for electrodeposition of dendrite-free zinc in an alkaline electrolyte modified with 1-ethyl-3-methylimidazolium dicyanamide. *Journal of Power Sources*, 274(2015), pp. 1249-1253.

Tan, I.A.W., Ahmad, A.L. and Hameed, B.H., 2008. Enhancement of basic dye adsorption uptake from aqueous solutions using chemically modified oil palm shell activated carbon. *Colloids and Surfaces A: Physicochemical and Engineering Aspects*, 318(1-3), pp. 88-96.

Tseng, H.H. and Wey, M.Y., 2006. Effects of acid treatments of activated carbon on its physiochemical structure as a support for copper oxide in $DeSO_2$ reaction catalysts. *Chemosphere*, 62(5), pp. 756-766.

Wendt, H. and Kreysa, G., 1999. *Electrochemical engineering: Science and Technology in chemical and other industries*. [e-book] New York: Springer. Available at: Google Books <books.google.com> [Accessed 14 July, 2014].

Winand, R., 2010. Electrodeposition of zinc and zinc alloys. In: M. Schlesinger and M. Paunovic, eds. *Modern electroplating*. 5th ed. [e-book] New Jersey: John Wiley & Sons, Inc. pp. 285-290. Available at: Google Books <books.google.com> [Accessed 23 July, 2014].

Yu, Y.D., Wei, G.Y., Lou, J.W., Ge. H.L., Sun, L.X. and Zhu, L.Z., 2013. Influence of bath temperature on zinc plating and passivation process. *Surface Engineering*, 29(3), pp. 234-239.

Zemanova, M. and Cocural, M., 2010. Corrosion resistance of pulse zinc coatings. In: G. Frankel, G. Grundmeier, H. McMurray and T. Shinohara, eds. *Coatings for corrosion protection*. [e-book] New Jersey: The Electrochemical Society. Available at: Google Books <books.google.com> [Accessed 7 July, 2014].

Zhang, X.G., 1996. *Corrosion and electrochemistry of zinc*. [e-book] New York: Plenum Press. Available at: Google Books <books.google.com> [Accessed 5 July, 2014].

APPENDICES

APPENDIX A: Calibration Results from ICP-OES

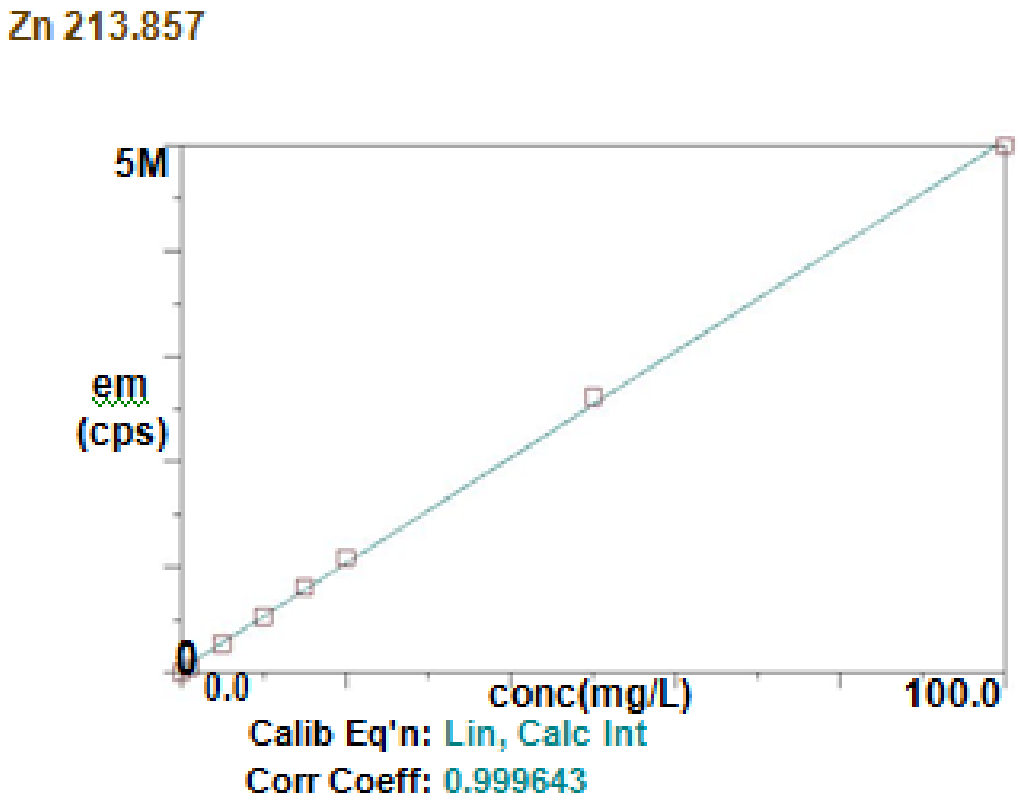

APPENDIX B: Zinc Concentration (ppm) and pH of Control Electrolyte

Time (min)	pH	Zinc Concentration (ppm)
0	0.28	6.784
5	0.29	7.551
10	0.30	7.546
15	0.26	7.588
20	0.24	7.519
25	0.24	7.513
30	0.23	7.103
35	0.23	7.870
40	0.22	7.913
45	0.22	8.141
50	0.22	8.165
55	0.17	8.445
60	0.18	8.381

APPENDIX C: Zinc Concentration (ppm) and pH of Electrolyte Containing $ZnCl_2$ and 1.0 M KCl

Time (min)	pH	Zinc Concentration (ppm)
0	0.34	9.514
5	0.38	9.600
10	0.39	10.160
15	0.34	9.755
20	0.33	9.577
25	0.34	4.904
30	0.30	6.645
35	0.28	3.622
40	0.28	6.347
45	0.26	4.466
50	0.26	3.774
55	0.24	5.250
60	0.24	3.597

APPENDIX D: Zinc Concentration (ppm) and pH of Electrolyte Containing $ZnCl_2$ and 0.5 M Boric Acid

Time (min)	pH	Zinc Concentration (ppm)
0	0.16	2.554
5	0.28	0.000
10	0.25	0.000
15	0.25	5.114
20	0.25	3.415
25	0.25	0.000
30	0.21	0.000
35	0.21	4.990
40	0.21	7.539
45	0.22	2.904
50	0.20	8.424
55	0.16	1.916
60	0.17	16.200

APPENDIX E: Zinc Concentration (ppm) and pH of Electrolyte at pH 4.5

Time (min)	pH	Zinc Concentration (ppm)
0	4.48	6.498
5	4.76	6.645
10	4.66	5.230
15	4.49	0.000
20	4.52	0.000
25	4.74	0.000
30	4.84	0.000
35	5.23	0.000
40	5.42	0.000
45	5.48	0.000
50	5.63	0.000
55	5.75	0.000
60	5.82	0.000

APPENDIX F: Zinc Concentration (ppm) and pH of Electrolyte at 45 ^{o}C

Time (min)	pH	Zinc Concentration (ppm)
0	0.54	6.751
5	0.45	7.466
10	0.54	8.360
15	0.50	8.748
20	0.46	8.615
25	0.49	7.078
30	0.42	7.333
35	0.48	7.111
40	0.45	7.283
45	0.46	7.679
50	0.32	7.685
55	0.31	7.645
60	0.41	7.255

APPENDIX G: Zinc Concentration (ppm) and pH of Electrolyte subject to Pulse Current

Time (min)	pH	Zinc Concentration (ppm)
0	0.17	6.342
5	0.28	7.172
10	0.28	7.489
15	0.27	7.762
20	0.28	7.173
25	0.25	6.665
30	0.27	7.615
35	0.25	10.420
40	0.25	7.915